Effective material usage in a compact heat exchanger with periodic micro-channels

Bertus George Kleynhans
B.Eng (Mechanical)

Mini-dissertation submitted in partial fulfilment of the requirements for the degree Master in Nuclear Engineering at the School of Mechanical and Nuclear Engineering, North-West University Potchefstroom Campus

Supervisor: Dr. J-H Kruger
Co-Supervisor: Prof. C.G. du Toit

Potchefstroom

2012

Acknowledgments

Thank You Lord Jesus Christ, without You none of this would have been possible.

Thank you, Marissa, my wife, for your love, support and patience.

Thank you, Evert and Monika Kleynhans, my parents, for all the opportunities and support you gave me.

Thank you, Prof. Jat du Toit and Dr. Jan-Hendrik Kruger, my study leaders, for your guidance, support and insight throughout the study.

Thank you, THRIP and NRF, for funding during my studies (2010 and 2011) whom without none of this would have been possible.

Oorsig

Titel : Effective material usage in a compact heat exchanger with periodic micro-channels

Skrywer : B.G. Kleynhans

Studieleiers : Dr. JH Kruger & Prof. C.G. du Toit

Skool : Skool vir Meganiese en Kern-Ingenieurswese

Graad : Meestersgraad in Kern-Ingenieurswese

Alle moderne hoë temperatuur, gas verkoelde, reaktor siklusse het een komponent in gemeen: een of ander vorm van ‘n hitteruiler in die primêre siklus. Die doel van so ‘n hitteruiler is om die werksvloeier te verhit of af te koel voordat dit deur die res van die reaktor siklus beweeg.

Kompakte plaat-tipe hitteruilers bied hoë hitte oordrag in kleiner volumes. Verskeie studies is gedoen om die hitte oordrag in vloeikanale te verbeter vir kompakte hitteruilers maar kleiner fokus is sover nog geplaas op die termiese ontwerp van die omliggende soliede materiaal.

Die fokus van hierdie studie is dus om ‘n metode te ontwikkel om die effektiewe materiaal gebruik in so hitteruiler te bevorder. Drie toetsgevalle is bestudeer (trapesium, trapvormige en sigsag uitlegte met half-sirkel) en al drie gevalle is onder dieselfde randvoorwaardes getoets. Die toetsgevalle is met Berekenings Vloei Meganika gesimuleer en die resultate geëvalueer met behulp van vier faktore naamlik, “heat spots”, “volume verhouding”, “temperatuur verskil”, en ‘n “verbeteringsfaktor”.

Die resultate het getoon dat die sigsag uitleg die beste presteer wanneer dit t.o.v. die bogenoemde faktore geëvalueer is terwyl die trapvormige uitleg die slegste presteer het, i.t.v. hitte-oordrag verbeterings.

Abstract

Title : Effective material usage in a compact heat exchanger with periodic micro-channels

Author : B.G. Kleynhans

Supervisors : Dr. JH Kruger & Prof. C.G. du Toit

School : School of Mechanical and Nuclear Engineering

Degree : Master in Nuclear Engineering

All modern High Temperature Reactors (HTR) thermal cycles have one thing in common: the use of some form of heat exchanger. This heat exchanger is used to pre-heat or cool the primary loop gas, from where the secondary power generation cycle is driven.

The Compact Heat Exchanger (CHE) type offers high heat loads in smaller volumes. Various studies have been done to improve the heat transfer in the flow channels of these CHEs but little focus has been placed on the thermal design of surrounding material in such a heat exchanger.

The focus of this study is on the effective material usage in a CHE. Three test cases were investigated (trapezoidal, serpentine and zigzag layouts with semi-circular cross-sections) all under the same boundary conditions. Computational Fluid Dynamics (CFD) was used to simulate these test cases and the results were evaluated according to four factors, the volume ratio, heat spots, temperature difference and the combined enhancement factor.

From the results it was concluded that the zigzag layout performs best when evaluated according to the volume ratio and the temperature difference and gave the best overall enhancement factor. The serpentine layout performed the worst when evaluated according to the enhancement factor.

Keywords:

Material usage, heat transfer enhancement, pressure-drop penalty, volume ratio, heat spots, temperature difference, serpentine, trapezoidal and zigzag.

Table of contents

List of figures

List of tables

List of acronyms

CAD	Computer Aided Design
CFD	Computational Fluid Dynamics
CHE	Compact Heat Exchanger
CS	Control Surfaces
CV	Control Volumes
DBHE	Diffusion Bonded Heat Exchanger
HPC	High Performance Computer
HTR	High Temperature Reactor
IHX	Intermediate Heat Exchanger
NRF	National Research Foundation
THRIP	Technology and Human Resources for Industry Programme
VC	Volume Cells

List of symbols

Symbols	Unit	Description
A	m	Amplitude
A_c	m^2	Flow cross-section
B	m	Length of top run
C_p	kJ/kg.K	Specific heat
d	m	Diameter
$\frac{d_p}{d_x}$	kPa/m	Pressure gradient
D_h	m	Hydraulic diameter
$\frac{d_T}{d_x}$	K/m	Temperature gradient
e_A	-	Area enhancement
e_f	-	Pressure-drop penalty
e_{Nu}	-	Heat transfer enhancement
h	W/m^2	Convection coefficient
i_A	-	Heat transfer intensification
k	W/m.K	Thermal conductivity
L	m	Half wavelength
l	m	Length of the channel
L_h	m	Hydraulic entrance length
L_t	m	Thermal entrance length
m_p	kg	Mass of particle
$\dot{m}$	kg/s	Mass flow rate of the fluid
Nu	-	Nusselt number
Nu_f	-	Nusselt number for straight flow path
Nu_s	-	Nusselt number for bended flow path
P	m	Wetted perimeter
p_{in}	Pa	Inlet pressure
p_{out}	Pa	Outlet pressure
Pr	-	Prandtl number
q''	W/m^2	Heat flux
Q_{rad}	kW	Radiative heat transfer
Q_s	kW	Heat from other sources
Q_t	kW	Convective heat transfer
r	m	Radius from centreline
R_c	m	Radius of bends
Re	-	Reynolds number
r_o	m	Outer radius of pipe
S	m	Path length
$T1$	K	High temperature
$T2$	K	Low temperature
t_{mi}	K	Mean temperature of fluid at inlet

t_{mo}	K	Mean temperature of fluid at outlet
t_{so}	K	Temperature of the surface of the solid at the outlet
T_{fluid}	K	temperature of passing fluid
T_p	K	Particle temperature
T_s	K	Surface temperature
T_∞	K	Fluid temperature
V	m/s	Mean velocity

Greek symbols	**Unit**	**Description**
α	Degrees	Deviation angle
ρ	kg/m^3	Density
μ	kg/m.s	Dynamic viscosity

1 Introduction

Heat exchangers are purpose built to transfer heat from one medium to another. They are widely used in numerous applications such as combustion engines, refrigeration, air conditioners and power plants. The fluids in the exchanger are usually separated in such a way that they never mix or come in contact with one another.

A variety of heat exchangers are in use but share a common goal: to exchange heat efficiently and effectively. The focus in this study was on one type of heat exchanger namely a Compact Heat Exchanger (CHE) which serves as an Intermediate Heat Exchanger (IHX) in power generation cycles. These types of heat exchanger are proposed for use in modern HTR power plants because of their high area density which results in more effective heat transfer with smaller exchangers. Because the IHX must be located within the primary containment, equipment must be designed for efficient use of physical volume.

There also exist various types of CHEs but the specific type investigated in this study is Diffusion Bonded Heat Exchangers (DBHE) also known as Micro-Channel Heat Exchangers (MCHEs). These types of exchangers consists of multiple layers of plates (alternating primary and secondary layers) which are diffusion welded to one another as illustrated in Figure 1.1. The primary layers carry the hot fluid while the secondary layers convey the cold fluid or vice versa. Manifolds are connected to the primary and secondary sides to ensure that the correct fluid stream enters the appropriate channel layer.

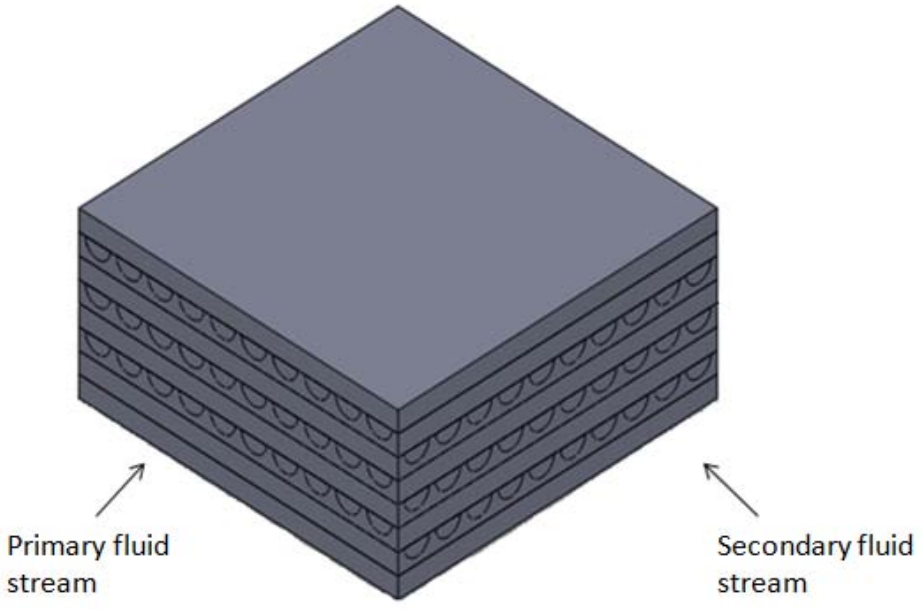

Figure 1.1 - Illustration of a typical MCHE

1.1 Problem statement

There currently exists numerous studies in terms of heat transfer enhancement, pressure losses and the stacking ability of the micro-channels but most were done using single channel simulations of only the flow domain. The effect of the temperature distribution on the surrounding material is not widely reported. The need originated to introduce the solid region to examine the total effect of not only the channel layout and its cross-section but also the effect that the shape of the surrounding solid has on the temperature distributions and the overall performance of the exchanger.

1.2 Objective of the study

The aim of this study was to examine the introduction of the surrounding solid material in the numerical model to determine its effect on the calculation of heat transfer and temperature distribution between multiple channels in the same plate layer.

Evaluation factors are introduced which describe the effectivity of the material usage, the temperature distribution variance and heat transfer enhancement. Fatigue-induced thermal stresses due to temperature gradients are the motivation behind the study, but a detailed description there-of does not fall under the scope of the study.

1.3 Chapter overview

In chapter 2 a literature survey is described that examined different micro-channel layouts with different cross-sections with regard to the heat transfer enhancement, pressure-drop penalty and the stacking ability of the different layouts. The fundamentals of heat transfer, flow associated phenomena, boundary conditions, mesh setups and an overview of CFD methodology are also given.

In chapter 3 the validation of the numerical model was conducted by modelling specific geometries and boundary conditions found in the literature and evaluating the results. The introduction of a conductive interface between the solid and fluid region was evaluated on whether heat transfer over the interface is predicted accurately in a conservative manner.

In chapter 4 new relations are defined which will be used to evaluate the results of the study. These factors are the volume ratio, so called “heat spots” and the enhancement factor. The methodology of the numerical study is also presented in this chapter.

Chapter 5 outlines how various configurations of the micro-channel pathways were investigated with the addition of solid material, all under the same flow conditions and heat transfer rates to investigate the influence of the solid region on the temperature distribution and volume ratios.

In chapter 6 the conclusions from this study are summarized together with recommendations for further study with regards to the expansion of this body of knowledge.

2 Literature survey

When using micro-channels in heat exchangers, numerous variations can be applied to the channel geometry and flow conditions to improve overall performance. These performance areas include, but is not limited to, heat transfer capabilities, pressure losses and stacking abilities for the various geometrical pathways or flow paths.

Analyses of these design options with regard to cross-section variations, flow path layouts, bend radii etc. were investigated and evaluated to determine which of these features are best altered to enhance the overall performance of MCHEs.

2.1. Duct shape effects

In a study by Erdoğan & Imrak (2005) the effect that the shape of the duct has on the Nusselt number has been considered. Four duct shapes were considered namely: semi-circular cross-section, circular cross-section, rectangular cross-section and flow between two parallel plates.

The effect of the heat transfer has been considered under laminar flow conditions and the results that were obtained are as follows:

Table 2-1 - Duct shape Nusselt numbers (Erdoğan & Imrak (2005))

Duct shape	Nusselt number
Semi-circular	4.088
Circular	4.363
Rectangular	3.549
Parallel plates	8.235

It was concluded that the duct shape has a significant effect on the relative Nusselt number. It can be noted from Table 2-1 how the Nusselt number under the same boundary conditions varies when the cross-section is changed.

2.2. Design features of micro-channels

Focus was placed on the simulation and setup of micro-channels within a single plate layer in a CHE. A micro-channel in this study is defined as a channel, which serves as the pathway for the fluid, which has a hydraulic diameter ≤ 3 mm. An investigation into the design features of sinusoidal and trapezoidal shape path ways with alterations in the layout geometries and the effects thereof will be described in more detail in the following sections.

2.2.1. Sinusoidal pathways

Periodic sinusoidal pathways were investigated by Rosaguti et al. (2007). The study was done using CFD, in terms of the heat transfer enhancement related to the relative pressure-drop penalty for circular and semi-circular flow cross-sections. The heat transfer enhancement and pressure-drop penalty will be described later in the literature survey.

2.2.1.1. Geometry of sinusoidal pathways

Sinusoidal shape pathways are one of the pathway layouts that can be used in MCHEs. The performance of this shape will be discussed in the sections to follow. The general shape of a sinusoidal channel is represented in Figure 2-1 with the geometric dimensions L, A and d

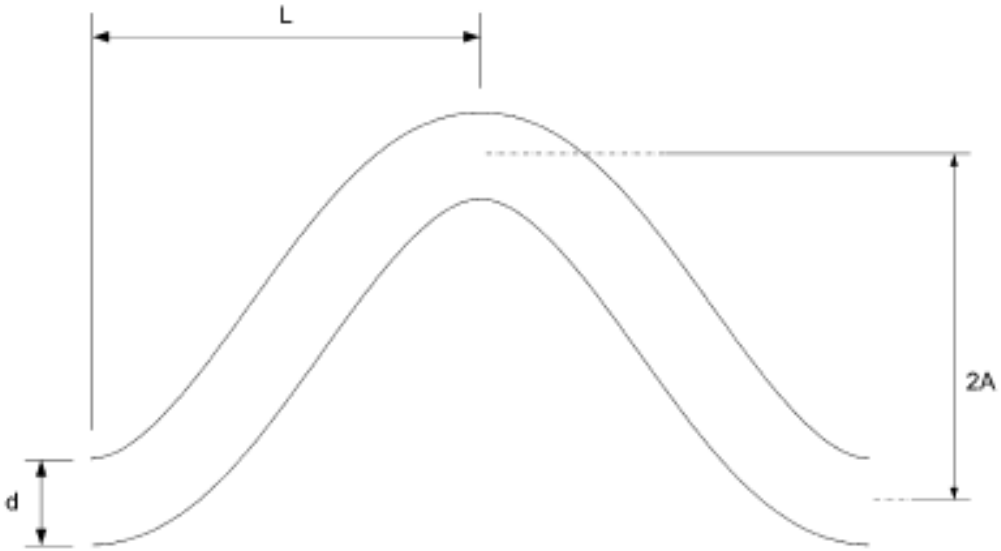

Figure 2-1 – General sinusoidal layout

where L, A and d represent the channel half wavelength, amplitude and the diameter respectively. In the next section it will become clear how the dimensionless relations can be altered to manipulate the layout. With an increase in the value of A/L the amplitude of the sinusoidal shape will become larger for the same period of the sinus wave and vice versa (Figure 2-3).

2.2.1.2. Previous work on sinusoidal pathways

In the study by Rosaguti et al. (2007), they reported on the effect of varying the Reynolds number (5 ≤ Re ≤ 200) and the non-dimensional ratio (0.222 ≤ A/L ≤ 0.667) with a constant ratio (L/d = 4.5) for fully developed laminar flow and at steady state, incompressible, constant property conditions for water (Pr = 6.13). The significance in the change of the A/L ratio can be seen in the next section.

This was done under two boundary conditions, namely the T and H2 boundary condition of Shah & London (1978). A detailed discussion of these boundary conditions is given in section 2.7. It was found that the flow field was increasingly dominated by secondary flow structures as the Reynolds number of the flow was increased and with an increase in the dimensionless A/L ratio. These vortices are responsible for significant heat transfer enhancement with a relative small pressure-drop penalty within the channel when compared to straight pathways.

2.2.1.3. Heat transfer enhancement and pressure-drop penalty for sinusoidal pathways

Results presented by Rosaguti et al. (2007) for a semi-circular flow cross-section are shown in Figures 2-2 to 2-4.

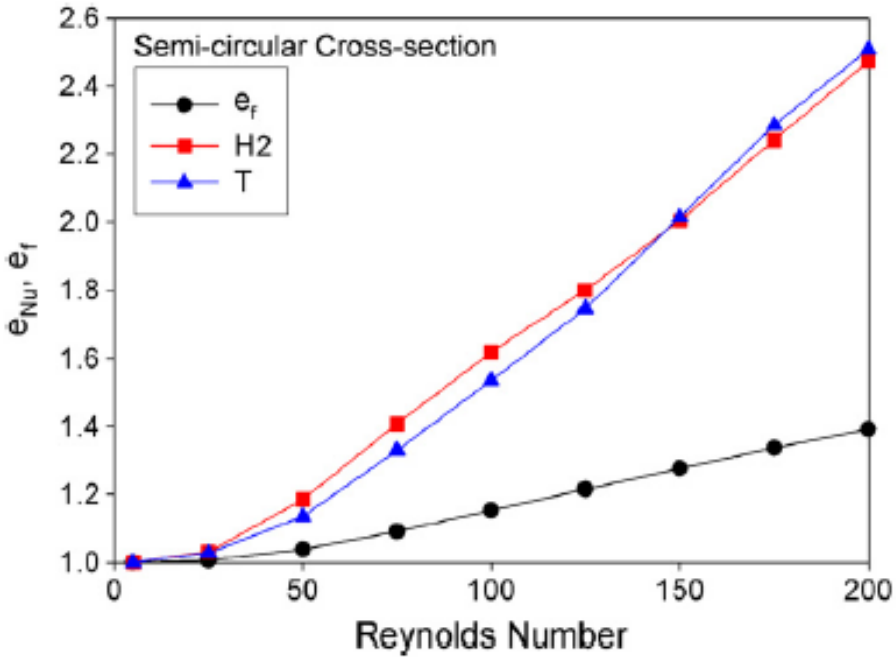

Figure 2-2 - Heat transfer enhancement and pressure-drop penalty as function of the Reynolds number (Rosaguti* et al.*, 2007)

The heat transfer enhancement, e_{Nu}, and the relative pressure-drop penalty, e_f, for various Reynolds numbers at both the H2 and T boundary conditions can be seen in Figure 2-2. The heat transfer enhancement and the pressure-drop penalty will be described in detail in section 2.5. It should just

be noted that a larger value in the heat transfer enhancement indicates better heat transfer and that a larger value in the pressure-drop penalty ratio indicates a larger pressure-drop over the channel.

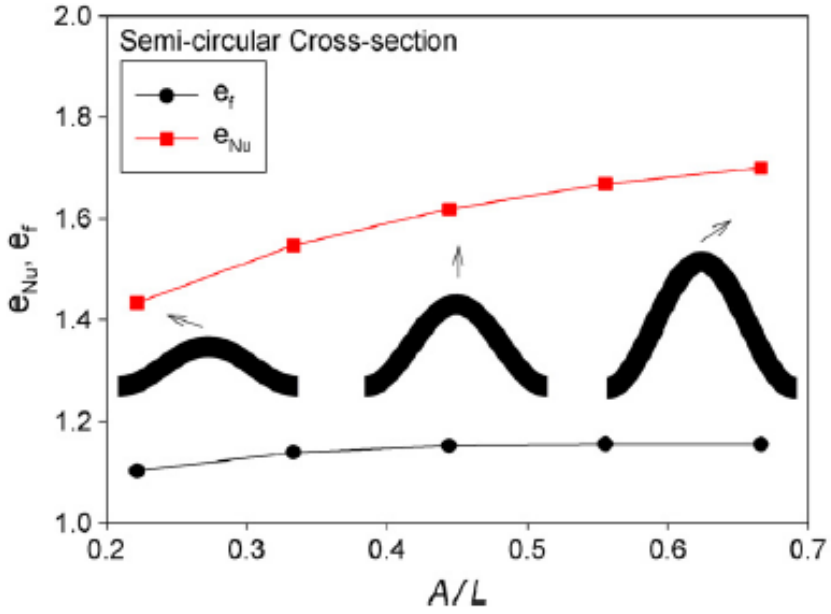

Figure 2-3 - Heat transfer enhancement and pressure-drop penalty as function of the A/L ratio (Rosaguti* et al.*, 2007)

Figure 2-3 represents the heat transfer enhancement and the pressure-drop penalty as a function of the change in the dimensionless ratio of A/L. As stated previously, the combined increases in the Reynolds number and the A/L ratio increase the magnitude of secondary flow structures. The effect of the dimensionless ratio on the heat transfer enhancement and the pressure-drop penalty can be seen in Figure 2-4, shown for various Reynolds numbers.

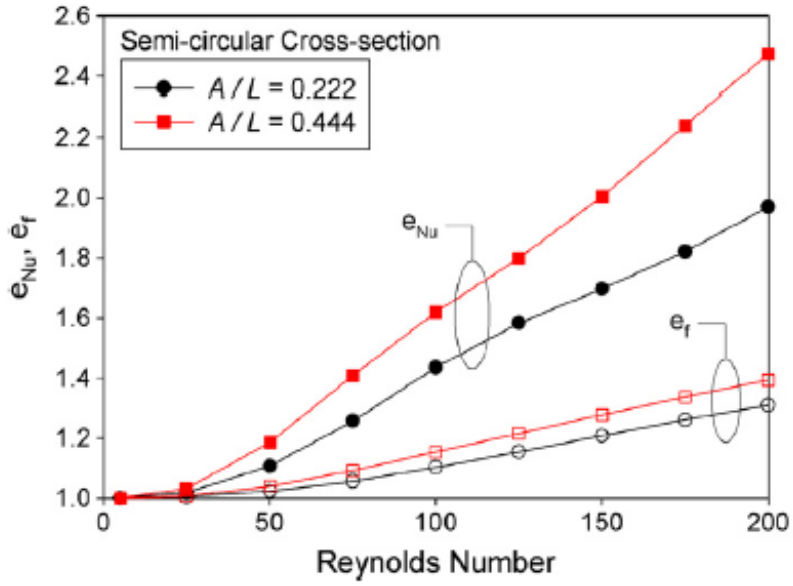

Figure 2-4 - Heat transfer enhancement and pressure-drop penalty as function of the Reynolds number for different A/L ratios(Rosaguti* et al.*, 2007)

Figure 2-4 represents two ratios (A/L = 0.222 and A/L = 0.444) as they were varied over a range of Reynolds numbers to illustrate the effect on the pressure-drop penalty and the heat transfer enhancement. It can be noted that with an increase in the Reynolds numbers, for a specified geometry, the secondary flow structures become more dominant and enhances the heat transfer ability of the fluid. As the Reynolds number increases, the fluid thus tends to mix more (this can be seen in section 2.4) but it also increases the pressure-drop within the channel.

2.2.1.4. Conclusion for sinusoidal pathways

Significant heat transfer enhancements balanced against relative small increases in pressure drops can be achieved with the slightest of changes in the geometry of the pathway. The heat transfer enhancement improves more in relative terms than the pressure-drop penalty increase with an increase in the amplitude (A/L ratio) and an increase in the Reynolds number.

2.2.2. Trapezoidal pathways

A trapezoidal flow path is another channel configuration that can be used in MCHEs. The defining differences between trapezoidal and sinusoidal layouts are that the “legs” of the pathways are straight and more practical to manufacture. Different permutations of the basic trapezoidal layout are possible, and described in this section. Studies with regards to the heat transfer enhancement and pressure-drop penalty for serpentine pathways were studied by Rosaguti et al. (2006). The heat transfer enhancement and pressure-drop penalty for trapezoidal pathways with triangular cross-sections was modelled by Gupta et al. (2008). The heat transfer enhancement, pressure-drop penalty and the stacking ability for trapezoidal pathways with semi-circular cross-sections were

investigated by Geyer et al. (2007). All of these studies were completed using commercial CFD software packages.

2.2.2.1. Geometry of trapezoidal pathways

The general shape of a trapezoidal pathway is represented by, Figure 2-5

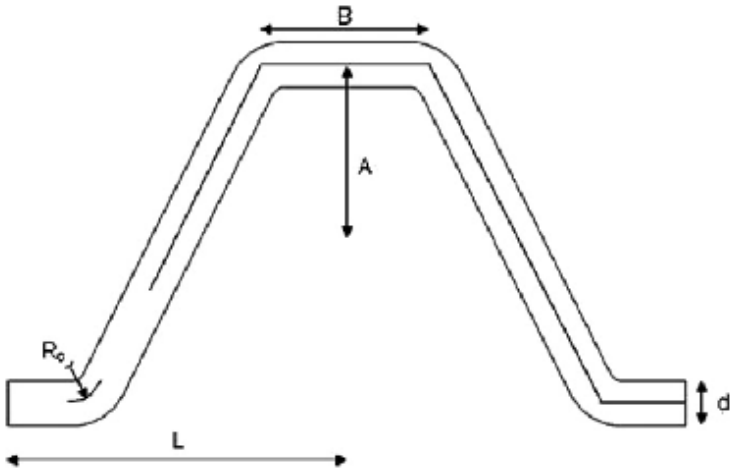

Figure 2-5 – General trapezoidal geometry (Geyer* et al.*, 2007)

where L is the unit half length, 2A is the height, R_c is the radius of the bends, d is the cross-section diameter and B is the length of the top run. The lengths of the diagonal sides are equal.

Different variations of the trapezoidal shape can be obtained through manipulation of the non-dimensional ratios. These shapes can vary from serpentine shapes to zigzag shapes as illustrated in Figure 2-6, Figure 2-7 and Figure 2-8. This is done by changing the non-dimensional ratios of B/L and A/L. The values for the ratios are tabulated in Table 2-2.

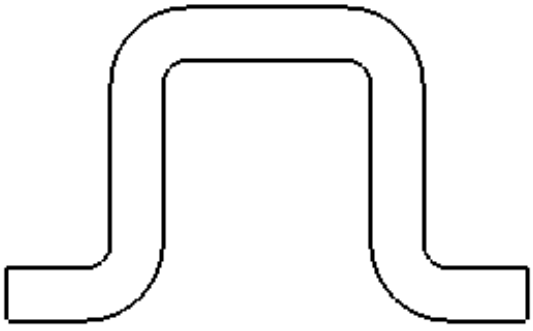

Figure 2-6 - Serpentine shape

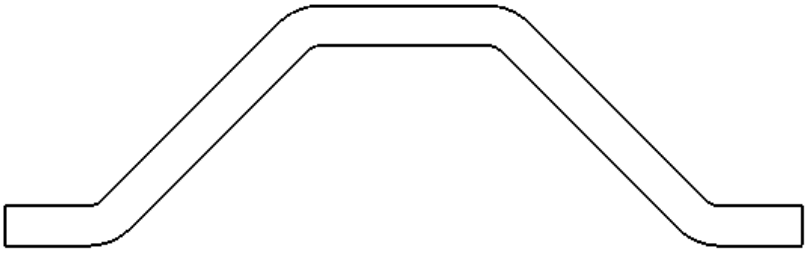

Figure 2-7 - Trapezoidal shape

Figure 2-8 - Zigzag shape

Table 2-2 - Trapezoidal ratios

Figure	Ratios	Values
Figure 2-6	B/L, A/L	1, 1
Figure 2-7	B/L, A/L	0.5, 0.5
Figure 2-8	B/L, A/L	0.2, 0.5

Table 2-2 presents examples of how the shape can be altered by changing a few of the dimensionless ratios. Results obtained for changes in the geometry will be discussed later in the literature survey.

2.2.2.2. Previous work on trapezoidal pathways

Comparative studies were done by Gupta et al. (2008) using different cross-sections (circular, semi-circular, square and triangular) with regard to the heat transfer enhancement and the pressure-drop penalty although the focus was more on the triangular cross-section.

Geyer et al. (2007) focussed only on a cross-section of semi-circular shape with regard to the heat transfer enhancement, pressure-drop penalty and the stacking ability of multiple micro-channels. The study was done for Re = 200 at a range of different geometric configurations ($0.525 \leq R_c \leq 1.3$, $3.6 \leq L/d \leq 12$, $0.17 \leq B/L \leq 1$, $0.125 \leq A/L \leq 1$). Geyer et al. (2007) considered the H1, H2 and T boundary conditions, which will be discussed later in the literature survey, for a fluid with a Prandtl number of 6.13.

As in the study done by Rosaguti et al. (2007), it was found that improved heat transfer enhancement was achieved using certain non-dimensional geometric configurations. The results due to these enhancements and the stacking ability of certain geometric configurations are discussed in the next section.

2.2.2.3. Results of trapezoidal pathways with regards to heat transfer enhancement and pressure-drop penalty

The results of heat transfer enhancement and pressure-drop penalty done by Geyer et al. (2007) for semi-circular cross-sections are represented in Figure 2-9 and Figure 2-10.

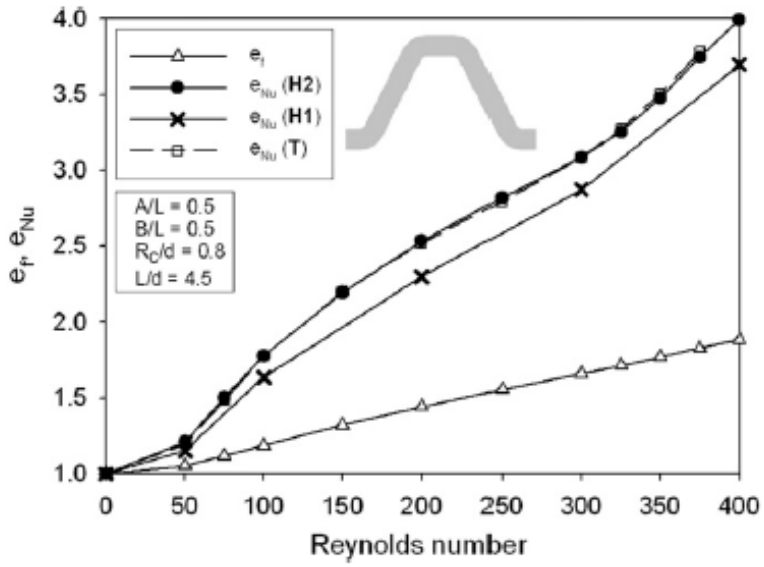

Figure 2-9 - Heat transfer enhancement and pressure-drop penalty as a function of the Reynolds number (Geyer* et al.*, 2007)

It should be noted in Figure 2-9 how the heat transfer enhancement coefficient and the pressure-drop penalty increase as the Reynolds number increase for the same geometrical layout. The same trends can be seen here as with the sinusoidal shape path ways, where the heat transfer enhancement improves more than the penalty in the pressure-drop.

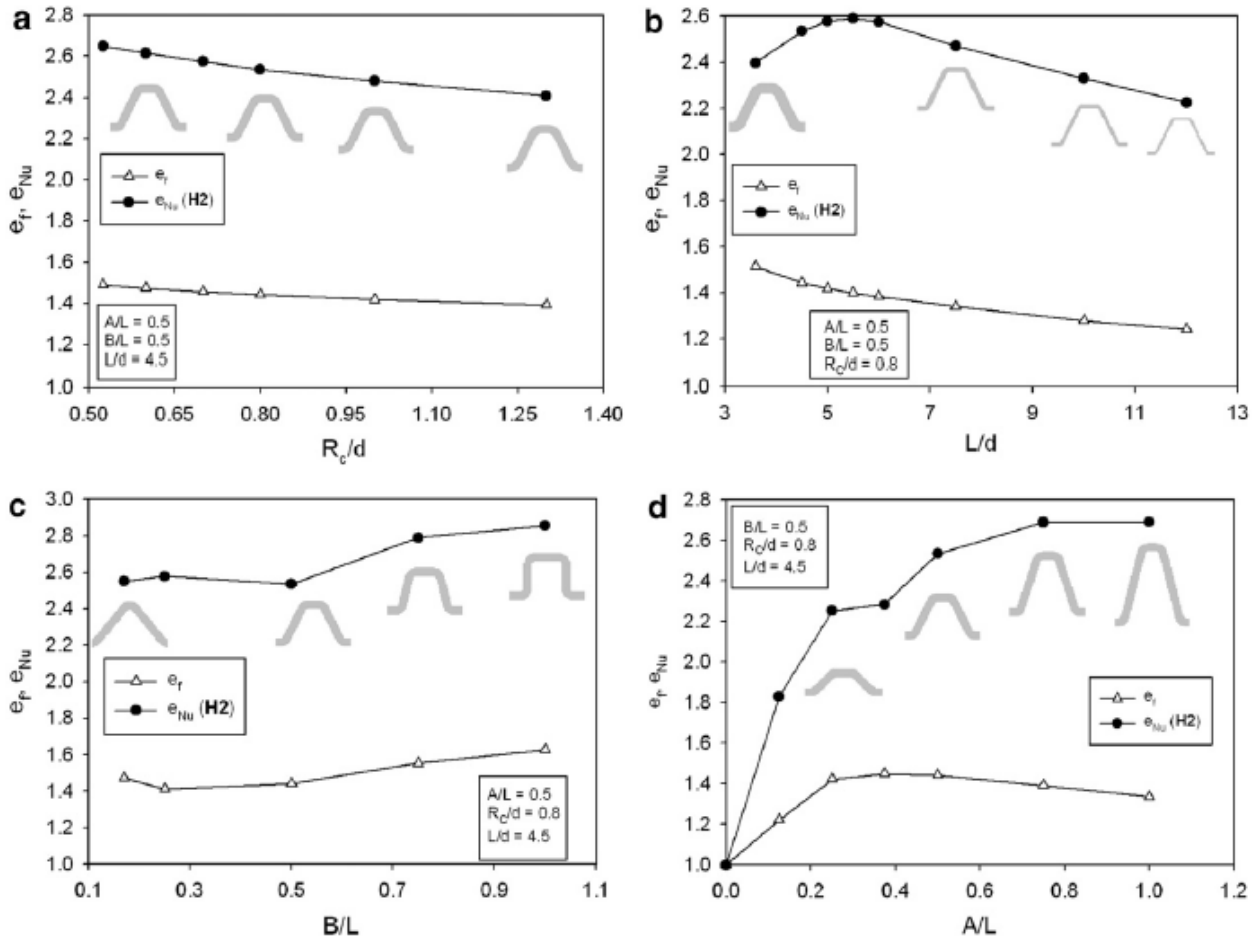

Figure 2-10 - Heat transfer enhancement and pressure-drop penalty for various geometric configurations at Re = 200 (Geyer* et al.*, 2007)

The results for single channel simulations in terms of the heat transfer enhancement and the pressure-drop penalty for the different boundary conditions, at various Reynolds numbers, (Figure 2-9) and different geometric configurations (Figure 2-10) can be seen. Figure 2-10 **a** – **d** represent the different geometric configurations for the non-dimensional ratios of R_c/d, L/d, B/L, and A/L. In Figure 2-10 the enhancements for the heat transfer and the increase in the pressure-drop penalty can be seen as functions of the non-dimensional ratios. The flow conditions for each case were kept the same and only the ratios were altered. It should be noted how the heat transfer enhances (larger values) and how it decreases with regards to the change in geometrical properties.

2.2.2.4. Conclusion for trapezoidal pathways

Trapezoidal pathways are yet another layout pattern that delivers an increase in the heat transfer capability of a CHE balanced with acceptable pressure-drop penalties. Some of the trapezoidal form variants also add value in the form of relatively good stackable possibilities. The stacking ability of trapezoidal shape pathways will become clearer later on in the study.

2.3. Solid region introduction

In the study by Kim et al. (2009) heat transfer was investigated between two channels in the primary and secondary layers. The temperature difference was measured at the inlets and outlets of both the hot and cold channels. The pressure drop through the hot and cold channels was also measured and compared with simulated data.

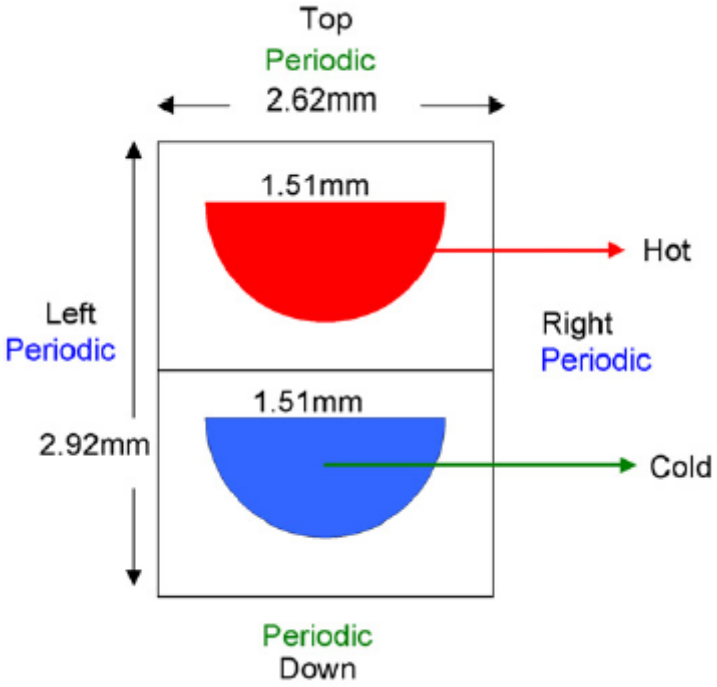

Figure 2-11 - Cross-section view of 3D simulation (Kim et al., 2009)

Figure 2-11 shows the cross-section view and approach, in terms of the boundary conditions, used in the simulation process. This study was conducted using zigzag periodic channels. Although multiple channels were simulated no detailed results were shown for the temperature distribution within the solid domain.

In the study by Mlcak et al. (2008), using a parallel array of micro-channels, heat transfer and laminar flow were studied numerically. A constant heat flux was applied to the computational domain and velocities, pressure and temperature were solved for.

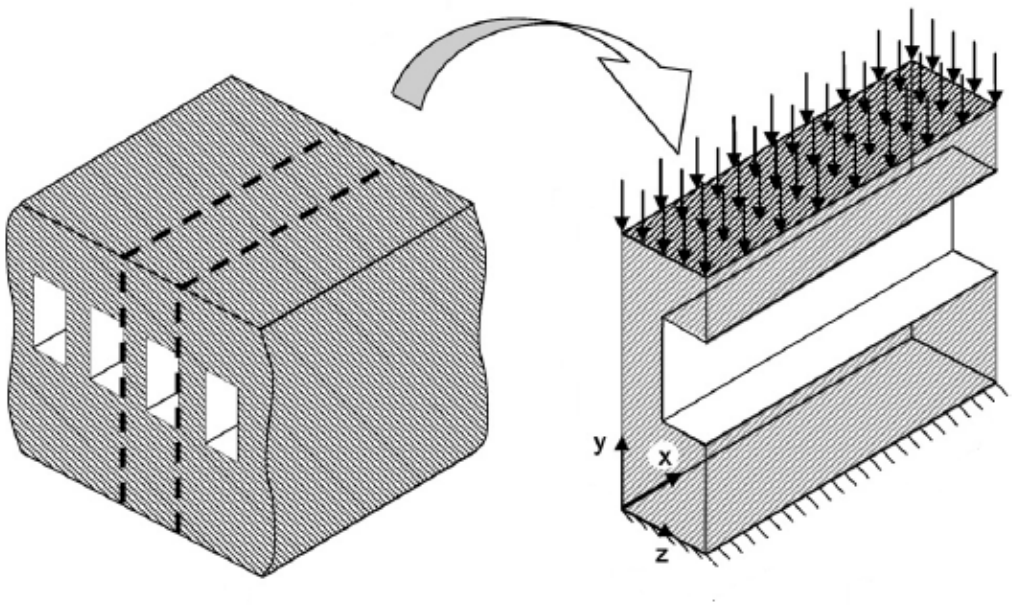

Figure 2-12 - Repeating micro-channel geometry (Mlcak et al., 2008)

Figure 2-12 shows the repeating geometry of the micro-channels. Although the solid region was added to the computational domain only a half channel was simulated due to the symmetry of the geometry. The numerical results at the inlet and exit of the channel matched the experimental measurements for the flow properties and temperature distribution.

In the study by Qu et al. (2000) the heat transfer characteristics were investigated for water flowing through a trapezoidal micro-channel, in both the solid and fluid regions. It was found that the experimental Nusselt number was much lower than the number given by the numerical analysis. It was suggested that the difference might be because of the surface roughness, and the effect thereof, within the micro-channel.

2.4. Flow regime

Although laminar and turbulent flow can be encountered in practice, focus in this study will only be on laminar flow as it is one of the typical design specifications for a CHE. In the study done by Venter (2010) on the pressure-drop penalty, it was recommended that the pressure drop through the channel should be kept as low as possible. In laminar flow the pressure-drop is less than that of turbulent flow, motivating the focus on laminar flow in the channels.

2.4.1. Fully developed flow

For flow to be considered fully developed, it must satisfy both conditions of thermally fully developed flow and hydraulically fully developed flow, according to Shah & London (1978).

These flow states are not strongly coupled to one another. This means that flow can be thermally fully developed and not hydraulically fully developed and vice versa. It is necessary for flow to be fully developed (hydraulic and thermal) to give suitable results when using numerical formulations valid for fully developed flow. For example the pressure drop per unit length within the entrance region is larger than the pressure drop in the fully developed region per unit length and that will have an adverse effect on the results when assuming fully developed flow in the complete region.

2.4.1.1. Hydraulically fully developed flow

Whenever flow enters a circular duct, the fluid is forced away from the wall and into the centre of the duct. This means that radial flow occurs for a certain distance from the entrance region. Eventually the boundary layer within the fluid extends towards the centre of the duct and for laminar flow the profile takes a parabolic shape in the hydraulically fully developed region. This can be seen in Figure 2-13.

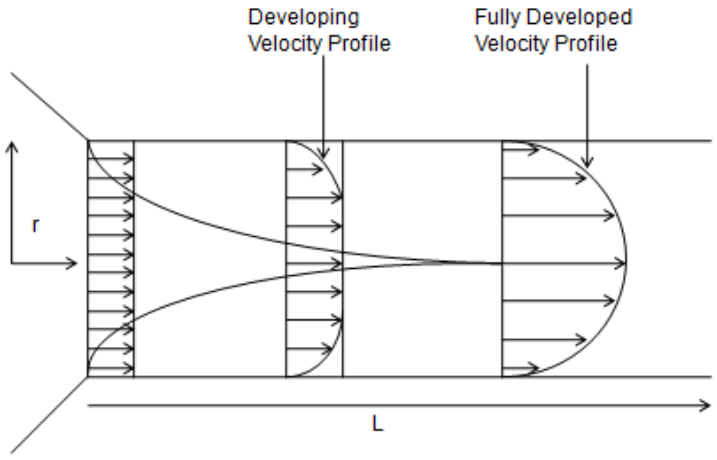

Figure 2-13 - Developing velocity profile

The point where the boundary layers meet is known as the hydraulic entrance length (L_h) and is defined by Kaminski & Jensen (2005) as:

$$L_h = 0.065 \times Re \times D_h \tag{2.1}$$

where *Re* is the Reynolds number of the fluid and D_h is the hydraulic diameter of the duct.

An equation to describe the velocity profile for laminar flow is given by Incropera *et al.* (2006) as:

$$u(r) = -\frac{1}{4\mu}\left(\frac{dp}{dx}\right) r_o^2 \left[1 - \left(\frac{r}{r_o}\right)^2\right] \tag{2.2}$$

where μ is the dynamic viscosity of the fluid, $\frac{dp}{dx}$ is the pressure gradient, r_o is the outer radius of the pipe and r is the radial position from the centre of the pipe.

2.4.1.2. Thermally fully developed flow

As in the case with the hydraulic boundary layer, the thermal boundary layer also develops from the entrance of the duct. The point where the boundary layers meet is known as the thermal entrance length (L_t) and is defined by Kaminski & Jensen (2005) as:

$$L_t = 0.037 \times Re \times Pr \times D_h \tag{2.3}$$

where *Pr* is the Prandtl number of the fluid.

2.4.2. Reynolds number

The Reynolds number, *Re*, is a dimensionless number that gives the ratio of the inertial to viscous forces in the velocity boundary layer which implies the ratio of momentum transport due to convection and diffusion. According to Munson & Young (2006) *Re* is defined as:

$$Re = \frac{\rho V D_h}{\mu} \tag{2.4}$$

where ρ is the density of the fluid, V is the mean velocity of the fluid and μ is the dynamic viscosity of the fluid.

The Reynolds number also gives an indication of the type of flow present, whether it is laminar or turbulent flow. In laminar flow the viscous forces are dominant and are characterized by a low Reynolds number ($Re \leq 2100$) where in turbulent flow the inertial forces are dominant and are typified by a high Reynolds number ($Re \geq 2300$).

2.4.3. Hydraulic diameter

The hydraulic diameter is defined in Incropera et al. (2006) as:

$$D_h = \frac{4A_C}{P} \tag{2.5}$$

where A_c is the flow cross-section and P is the wetted perimeter.

Equation (2.5) reduces to D_h = d (where d is the diameter of the pipe) for a circular cross-section (pipe) that is totally filled with a fluid and $D_h = \frac{d}{1+\frac{2}{\pi}}$ for a semi-circular flow cross-section.

2.5. Heat transfer

According to Kaminski & Jensen (2005) heat is transferred whenever there is a temperature difference between two points in a substance. These substances include solids, liquid, gas or plasma. The rate or the amount of heat transfer that occurs in the substance depends on the magnitude of the thermal resistance between the two points (Kaminski & Jensen, 2005). There exist three fundamental forms of heat transfer namely conduction, convection & radiation. Only conduction and convection will be discussed in this literature survey as radiation heat transfer falls outside the scope of this study.

2.5.1. Conduction

Conduction can be described as the diffusive transfer of energy in substances from a more energetic state to a less energetic state (Incropera *et al.*, 2006). This takes place on a molecular level where molecules vibrate faster in the more energetic state and thus have more energy (in this case higher temperature) and the energy is transferred through molecular motion to the less excited state. Conduction will take place where there exists a temperature gradient within the substance as shown in Figure 2-14.

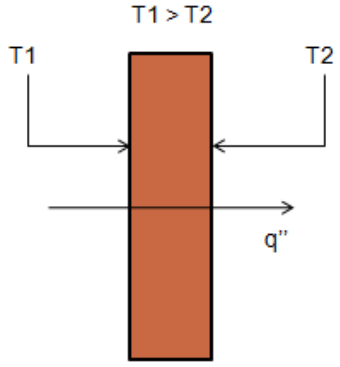

Figure 2-14 - Conduction

It can be seen from Figure 2-14 that the heat is transferred from a higher temperature (T1) to a lower temperature (T2) via conduction.

It is possible to express conduction in terms of an equation. The rate equation for heat conduction is known as *Fourier's law* and is expressed by Incropera et al. (2006) as

$$q_x'' = -k\frac{dT}{dx} = -k\frac{T_2 - T_1}{L} \tag{2.6}$$

for a one-dimensional plane where q_x'' (the heat flux in W/m^2) is the heat transfer rate in the *x* direction, k is the thermal conductivity (W/m • K) and $\frac{dT}{dx}$ is the temperature gradient present.

2.5.2. Convection

Two mechanisms make up convective heat transfer. This is energy transfer due to molecular diffusion and energy transfer due to the bulk motion of the fluid, according to Incropera et al. (2006). Whenever a moving fluid, whether a liquid or a gas, flows over a solid surface, which is at a different temperature than the fluid, convective heat transfer will take place (Kaminski & Jensen, 2005). The energy transfer due the motion of the fluid is illustrated in Figure 2-15.

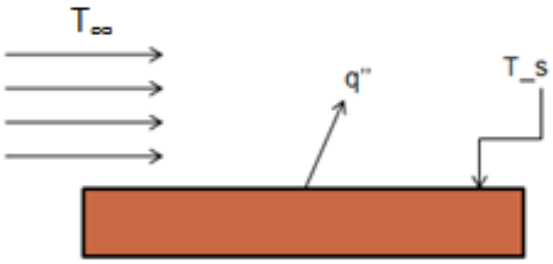

Figure 2-15 - Convection

The appropriate rate equation for convection is given, according to Incropera et al. (2006), by

$$q'' = h(T_s - T_\infty) \tag{2.7}$$

where q'' (W/m^2) is the convective heat flux per unit area, T_s is the surface temperature, T_∞ is the average bulk fluid temperature and *h* is the convective heat transfer coefficient.

2.5.3. Nusselt number

The Nusselt number is a non-dimensional heat transfer coefficient that indicates the ratio of convective to conductive heat transfer for fluids. The Nusselt number based on the hydraulic diameter is defined by Incropera et al. (2006) as

$$Nu = \frac{hD_h}{k} \tag{2.8}$$

where *h* is the convective heat transfer coefficient of the solid and *k* is the conduction coefficient (thermal conductivity) of the fluid. Higher Nusselt numbers imply higher rates of convective heat transfer between the fluid in the channels and the solid surrounding the passages. In the fully developed region (thermally and hydraulically) the convection heat transfer coefficient becomes constant, independent of the axial distance from the fully developed region.

2.5.4. Prandtl number

The Prandtl number relates the ability of a fluid to transport momentum to its ability to transport energy through diffusion in the velocity and thermal boundary layers respectively.

The Prandtl number is defined by Lamarsh & Baratta (2001) as

$$Pr = \frac{\mu C_p}{k} \tag{2.9}$$

where μ is the dynamic viscosity of the fluid and C_p is the specific heat of the fluid.

The Prandtl number is also used to characterize the formation of the thermal boundary layer as can be noted in equation (2.3). A large value for the Prandtl number implies that the velocity boundary layer will grow much faster than the thermal boundary layer and vice versa.

2.5.5. Heat transfer enhancement

The heat transfer enhancement is defined as

$$e_{Nu} = \frac{Nu_f}{Nu_s} \tag{2.10}$$

where Nu_f is the Nusselt number for the torturous flow path channel with a path length equal to that of a straight path and Nu_s the Nusselt number for a straight channel (Rosaguti *et al.*, 2006).

In effect this then gives a ratio of how much the heat transfer is enhanced (or reduced) with enhancements giving values larger than 1 and where deterioration occurs it results in a value of less than 1.

2.5.6. Pressure-drop penalty

The pressure-drop penalty works on the same basis [the pressure drop in a curved channel versus the pressure drop in a straight channel] as the heat transfer enhancement. The pressure-drop penalty is defined as

$$e_f = \frac{(p_{in} - p_{out})_{flowpath}}{(p_{in} - p_{out})_{straight}} \tag{2.11}$$

where p_{in} and p_{out} are the area-averaged inlet and outlet pressures respectively (Rosaguti *et al.*, 2006).

2.5.7. Area enhancement

The area enhancement factor is based solely on geometric factors with regards to the stacking ability of the inspected geometry (Geyer *et al.*, 2007). The stacking abilities of the various geometric layouts refer to how well multiple channels can be placed periodically alongside each other in the same plate layer to increase the area density. In chapter 4 multiple channels will be "stacked" and the impact of the stacking abilities will become clearer. Chapter 4 will also illustrate which geometries stack well and those geometries that do not.

The area enhancement factor, e_A, is defined as

$$e_A = \frac{S \cdot \cos\alpha}{2L} \tag{2.12}$$

where *S* is the path length of one period of the layout, α is the angle of deviation (Figure 2-16) of the side of the trapezoid and *2L* is the wavelength of the geometry (Geyer *et al.*, 2007).

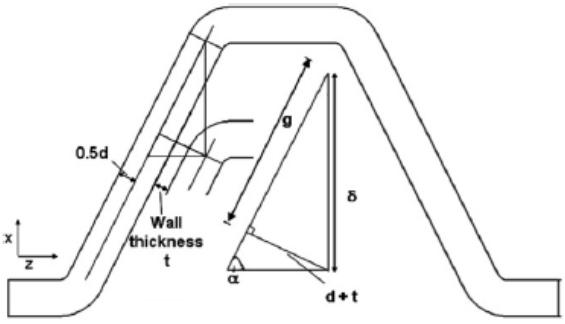

Figure 2-16 - Trapezoidal Configuration (Geyer* et al.*, 2007)

Figure 2-16 shows the configuration used in Equation (2.12) with regards to the angle of deviation.

2.5.8. Heat transfer intensification

The heat transfer intensification according to Geyer et al. (2007) is defined as

$$i_A = e_{Nu} \cdot e_A \tag{2.13}$$

where e_{Nu} is the heat transfer enhancement and e_A is the area enhancement factor.

It should be noted that heat transfer intensification is the product of the heat transfer enhancement and the area enhancements. Geyer et al. (2007) investigated heat transfer intensification and obtained the results displayed in Figure 2-17.

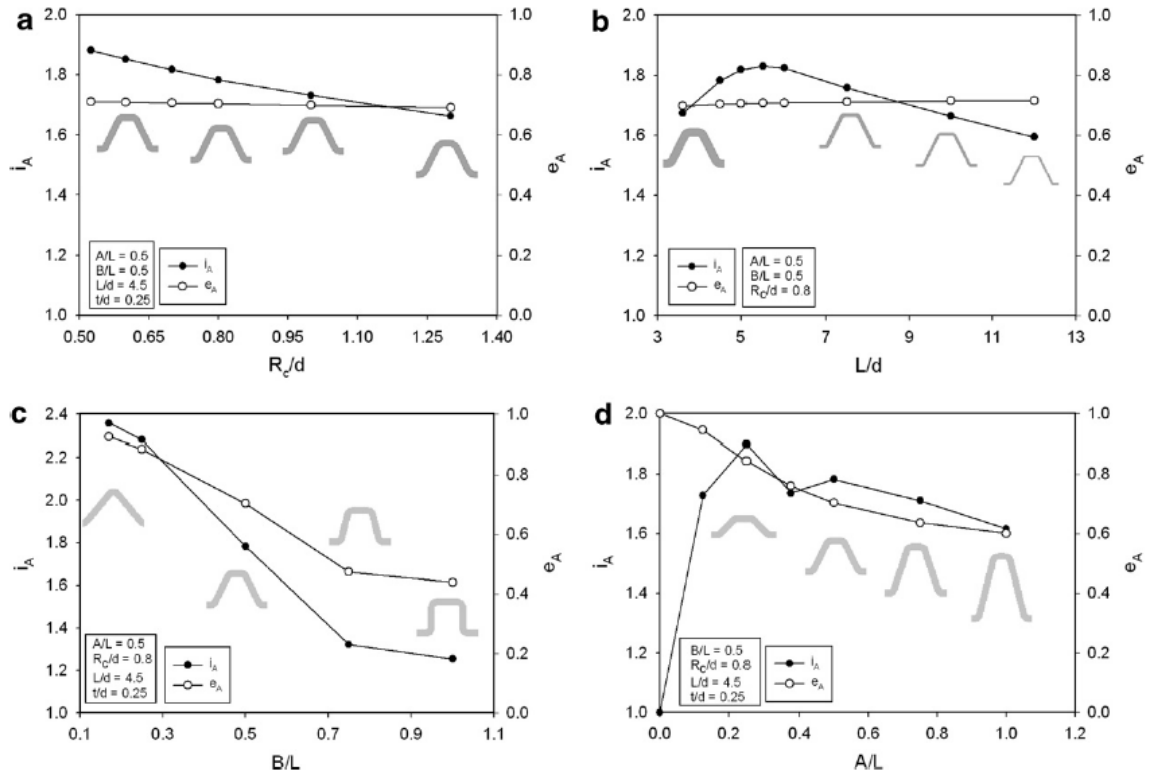

Figure 2-17 - Heat transfer intensification (Geyer* et al.*, 2007)

The heat transfer intensification, as a function of the various dimensionless ratios, is illustrated in Figure 2-17 **a**-**d**. In each figure only one ratio is altered (while the others are kept constant) and the effect (heat transfer intensification) thereof is presented on the y-axis of the graphs. Based solely on the geometry of the path way this gives a good indication of which ratios stack better than others. In chapter 4 the stacking abilities of these various geometric layouts will become clearer as the non-dimensional ratios will be altered to illustrate this property.

2.6. Introduction to CFD

According to Versteeg & Malalasekera (2007) CFD is a set of numerical techniques that are used in the numerical analysis of systems. These systems contain phenomena that include heat transfer, fluid flow and associated phenomena such as chemical reactions. The technique is very powerful and can be applied over a wide range of applications, industrial and non-industrial to obtain detailed insight into process behaviours. Some examples where CFD can be applied where in-depth experimental measurements are difficult, very expensive or impossible are:

- Aerodynamics of vehicles, aircrafts and buildings
- Hydrodynamics of pumps and ships
- Internal combustion engines
- Turbo machinery
- Weather predictions
- Fluid flow and neutronics inside nuclear reactors
- Heat transfer and fluid flow inside CHEs

STAR-CCM+ solves the governing physics equations using a *finite-volume* based method. The physical domain that is being investigated is represented by smaller non-overlapping Control Volumes (CV) of which the outer surface of each CV is its Control Surface (CS). The governing equations are applied to each CV and together with the boundary conditions form a system of simultaneous algebraic equations that are solved for all the CVs in the domain. The governing equations consist of the equations for the conservation of mass, momentum and energy.

The conservation of mass is described by

Rate of mass increase of the fluid inside the CV= Net rate of mass flow into the CV

and is defined by Munson & Young (2006) as:

$$\frac{\partial}{\partial t}\int_{CV}\rho d\psi + \int_{CS}\rho \boldsymbol{V}\hat{\boldsymbol{n}}\, dA = 0 \tag{2.14}$$

where $\hat{\boldsymbol{n}}$ is the unit vector perpendicular to the CS and $\boldsymbol{V}$ is the local velocity vector of the mass. Equation(2.14) states that to conserve mass, the rate of change of the mass of the CV must equal the net rate of mass flow through the CS. Equation (2.14) is called the *continuity equation*.

The conservation of momentum is described by

Rate of momentum increase of fluid in the CV = Sum of forces acting on the fluid in the CV

and is defined from Munson & Young (2006:206) as:

$$\frac{\partial}{\partial t}\int_{CV} \boldsymbol{V}\rho d\psi + \int_{CS} \boldsymbol{V}\rho \boldsymbol{V}\cdot\hat{\boldsymbol{n}}\, dA = \sum \boldsymbol{F}_{\substack{contents\ of\ the \\ control\ volume}} \tag{2.15}$$

where $\sum \boldsymbol{F}$ is the sum of forces that are acting on the fluid. Equation (2.15) states that the increase/decrease in momentum of the fluid in a CV is equal to the forces acting on the fluid in the CV. Equation (2.15) is called the *linear momentum equation*.

The conservation of energy in the CV is described by

Rate of energy increase of fluid = Net rate of added heat + net rate of work done on fluid

and is taken from Munson & Young (2006:230) as:

$$\frac{\partial}{\partial t}\int_{CV} e\rho d\psi + \int_{CS} e\rho \boldsymbol{V}\cdot\hat{\boldsymbol{n}}\, dA = (\dot{Q}_{\substack{net \\ in}} + \dot{W}_{\substack{net \\ in}})_{CV} \tag{2.16}$$

where e is the total stored energy per unit mass, $\dot{Q}$ is all the possible ways energy or heat is exchanged with the CV and $\dot{W}$ is the work done on the fluid, also called *power*.

The equation for the conservation of energy in the solid region is given by CD - Adapco (2011) as:

$$m_p c_p \frac{dT_p}{dt} = Q_t + Q_{rad} + Q_s \tag{2.17}$$

where m_p is the mass of the control volume, c_p is the specific heat of the CV, $\frac{dT_p}{dt}$ is the rate of change of the temperature, Q_t is the convective heat transfer to the CV, Q_{rad} is the rate of radiative heat transfer and Q_s represent other heat sources.

This then concludes the overview of important equations used in CFD modelling. As mentioned the above governing equations are discretized and solved for each of the CVs. This is the basis by

which the *finite volume* method is used to calculate solutions across a complete domain within STAR-CCM+.

2.6.1. Meshing cell types available in STAR-CCM+

The numerical volume meshes for STAR-CCM+ can contain the following types of computational cells, which are used in different combinations to optimally discretize a flow/solid region:

- Trimmed cells
- Polyhedral cells
- Tetrahedral cells

Some of the characteristics for the core volume meshes will be summarised in the next table.

Table 2-3 – Meshing characteristics (CD-adapco, 2011)

	Characteristics
Trimmed	• Provides high quality grid through robust and efficient cells (based upon numerically well behaved hexagonal cells) • Suitable for simple and complex geometries • Limited to one region
Polyhedral	• Efficient and easy to generate • Contains more or less 5 times fewer cells than a tetrahedral mesh starting from the same surface • Numerical behaviour falls between trimmed and tetrahedral cells • Allows for multi-region meshes with a combined interface
Tetrahedral	• Provides an simple and efficient meshing solution for complex simulations

	• Uses the least amount of computational resources for a given number of computational cells • Can result in very ill-formed cells with undesirable numerical behaviours • Multi-region meshes with an interface are allowed

In addition to the core volume meshing tools, prism layers, an extruded mesh and symmetry plane can be used to describe the numerical domain.

Prism layers generate orthogonal prismatic cells next to a selected geometry surface. This is usually used to accurately simulate boundary phenomena related to heat transfer or fluid flow.

The extruded mesh can be formed from the core volume mesh surface to produce orthogonal extruded cells for a selected boundary surface. The extruded mesh is typically used to extend the inlet or outlet of an existing volume mesh, to create longer inlet/outlet sections for better flow development.

In the simulation process symmetry planes can be used to reduce the computational cells needed to calculate a model. This however is limited by symmetry, if the problem does not feature symmetrical phenomena distributions inaccurate results will be obtained when using a symmetry plane.

2.7. Boundary conditions

To solve the governing equations boundary conditions need to be specified. These boundary conditions include thermal, flow (laminar or turbulent) and inlet or outlet conditions. In this chapter the focus will be on the thermal boundary conditions as applied to the models which will be used to validate the modelling process using the STAR-CCM+ software package.

The boundary conditions that were selected for the validation process is called the T and H2 boundary conditions from Shah & London (1978). These conditions with their description and proposed applications are given in Table 2-4 along with other conditions from the same reference.

Table 2-4 - Thermal boundary conditions for developed and developing flow in ducts (Shah & London: 1978)

Designation	Description	Application
T	Constant wall temperature peripherally as well as axially	Condensers, evaporators, automotive radiators (at high flows), with negligible wall thermal resistance
T3	Constant axial wall temperature with finite normal wall thermal resistance	Same as those for T with finite wall thermal resistance
T4	Nonlinear radiant-flux boundary condition	Radiators in space power systems, high-temperature liquid-metals facilities, high-temperature gas flow systems
H1	Constant axial wall heat flux with constant peripheral wall temperature	Same as those for H4 for highly conductive materials
H2	Constant axial wall heat flux with uniform peripheral wall heat flux	Same as those for H4 for very low conductive materials with the duct having uniform wall thickness
H3	Constant axial wall heat flux with finite normal wall thermal resistance	Same as those for H4 with finite normal wall thermal resistance and negligible peripheral wall heat conduction
H4	Constant axial wall heat flux with finite peripheral wall heat conduction	Electric resistance heating, nuclear heating, gas turbine regenerator, counter flow heat exchanger

2.8. Literature study conclusion

Selections of studies investigating micro-channels were discussed within the literature study. This included sinusoidal and trapezoidal shaped geometries with their respective performance studies. It was clear that the inclusion of bends in the pathway enhances the heat transfer but results in a larger pressure-drop penalty. The area enhancement was investigated by previous researches but based solely on the geometry of a single channel and not on multiple channel configurations, and was investigated in more detail in the current study.

All the major phenomena associated with the flow and heat transfer were discussed in sections 2.4 and 2.5. The boundary conditions used to validate the study, and an introduction to the numerical solver used in the simulations were also discussed.

The core volume meshes supplied by STAR-CCM+, their characteristics and a few usable meshing tools were briefly discussed.

The next chapter describes the validation process of the simulation methodology used with regards to the boundary conditions applied and the introduction of the solid region surrounding the fluid pathways.

3 Validation of the simulation methodology

This chapter focuses on the validation of the simulation methodology applied in this study using the software package STAR-CCM+. It is necessary to ensure that the specified software can be used to accurately simulate the test cases investigated in this study. The boundary conditions applied were the *T* and *H2* cases and comparisons were made with results from the literature with regards to the Nusselt number and the velocity profile, in the channel.

The introduction of solid material surrounding the channel requires a modelling interface between the fluid and the solid. The interface plays an important role as all the heat transfer takes place across the interface which acts as the numerical connection between the fluid and the solid regions. The validation process for the interface usage will be explained later in the chapter.

The Computer Aided Drawings (CAD) models for the two cases (both *T & H2* boundary conditions) are presented by Figure 3-1.

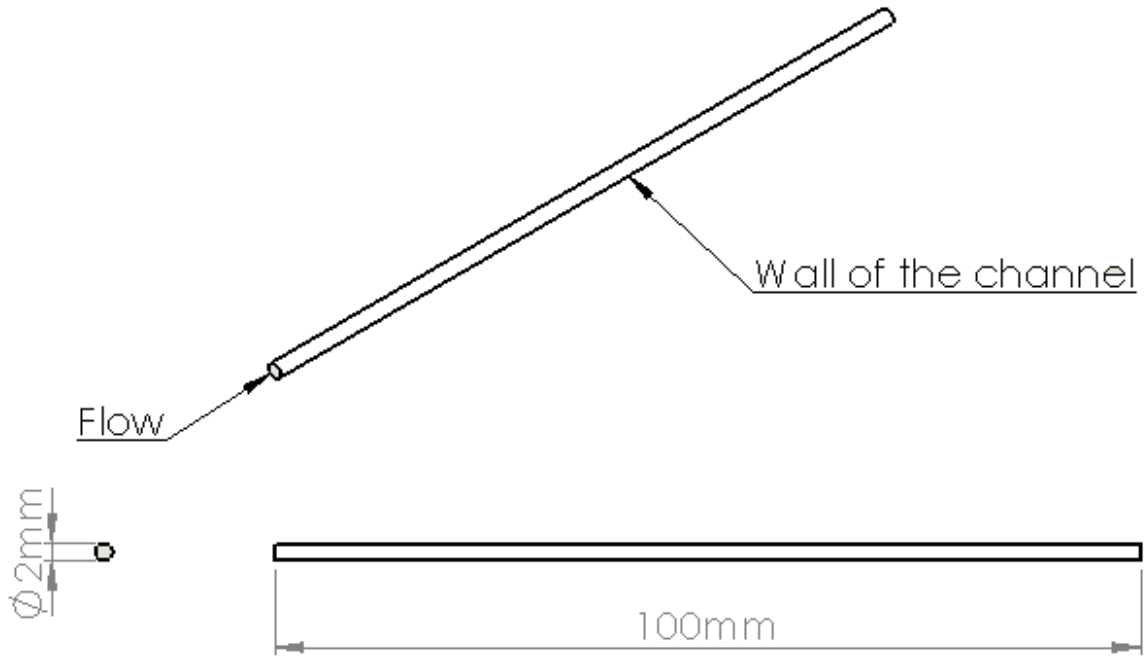

Figure 3-1 - CAD models for validation purposes

The wall of the channel, as indicated in Figure 3-1, is where the *T* and *H2* boundary conditions were applied in the two cases to follow.

3.1. Choice of mesh setup

Due to the limitations of certain meshing tools available from STAR-CCM+ (as explained in paragraph 2.6.1), the geometric layout of the final test cases and the availability of the High Performance Computer (HPC), the mesh setup used will be as follows:

The polyhedral meshing tool with the integrated prism layer tool will be used to generate the core volume mesh. It was determined by Venter (2010:23) that 4 prism layers (prismatic cells) at the wall of the channel are sufficient enough to deliver accurate results in the boundary layer region.

The extruder meshing tool can only be used as an “add-on” to the core volume mesh to extend, typically the inlet or the outlet, of the computational domain. It is also limited to simple geometries (extrusions along straight vectors) and cannot be used in complicated geometries (as in the final test cases).

Using a symmetry plane is dependent on the distribution of phenomena if it is usable or not. This feature will be illustrated later in the chapter.

The advantages of an extruded mesh and symmetry plane (if usable) are that fewer computational cells are needed and that faster solutions speeds can be obtained.

Thus, as mentioned, and for numerical consistency throughout the study the core volume mesh will consist of a polyhedral mesh with prismatic cells for boundary associated phenomena. This setup will be used in all the following cases with the exception of one symmetry plane model. The mesh properties will be presented later in this chapter.

3.2. Mesh independency (*T* boundary condition)

This section describes the *T* boundary condition. A mesh independency study was done to establish the number of volume cells (VC) needed to obtain sufficiently accurate results.

The boundary conditions and the fluid properties (steady state) for this case (circular duct) are as follows:

Table 3-1 - T boundary (Properties)

Properties	**Value**
Specific heat (C_p)	4183 J/kg-K
Density (ρ)	996.6 kg/m^3
Dynamic viscosity (μ)	0.0008542 kg/m-s
Thermal conductivity (k)	0.6203 W/m-K
Hydraulic diameter (D_h)	2 mm
Length (L)	100 mm
Reynolds number (Re)	100 (-)
Prandtl number (Pr)	5.761 (-)
Inlet velocity	0.04286 m/s
Inlet temperature	300 K
Wall temperature	350 K

This set of values was chosen to ensure that fully developed flow was achieved and so that results correlate with the literature.

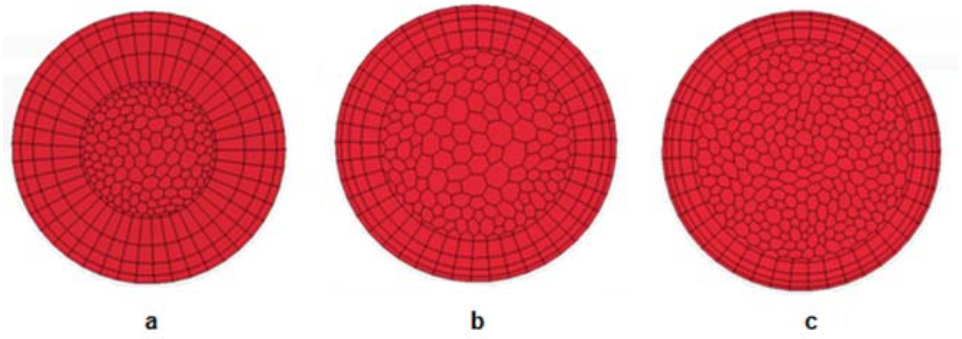

Figure 3-2 - Inlet region meshes

Figure 3-2 represents the 3 mesh resolutions used for the mesh independency study and the properties are given in Table 3-2. As stated in Table 3-1 the boundary conditions for all 3 mesh setups are the same with the only variation being in the mesh resolution (number of VCs).

***Table 3-2 - T* boundary (Results)**

#	**Base Size**	**Prism Layer Thickness (Fixed at 10% base size)**	**Volume Cells**	**Nusselt (*T*)** (Incropera *et al.*, 2006)	**Nusselt (L_t)**	**Error**
a	5mm	0.5mm	149880	3.66	3.308	9.6%
b	3mm	0.3mm	230584	3.66	3.405	6.9%
c	2mm	0.2mm	643721	3.66	3.69	0.81%

From Table 3-2 the variation in the results for the Nusselt number can be seen as the number of volume cells are increased and the thickness of the prism layers decreased. This clearly shows dependence of the accuracy of the simulation on mesh resolution. The Nusselt number (Nusselt (L_t)) presented in Table 3-2 was calculated at the point where flow within the channels was fully developed. From the definition in section 2.2.1 this is where the flow is hydraulically and thermally fully developed and using equation (2.3) it occurs at L_t = 0.04263 m. Figure 3-3, Figure 3-4 and Figure 3-5 represent the variation in the Nusselt number (for the three cases) as the flow develops through the channel until it is fully developed.

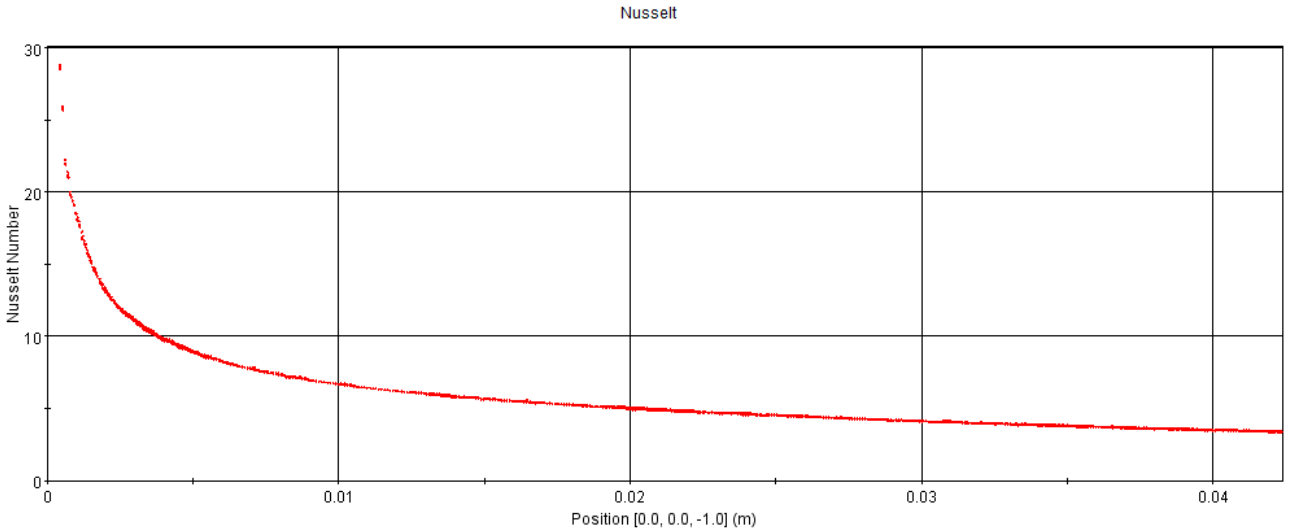

Figure 3-3 - Nusselt number for case a (T)

From Shah & London (1978) it states that the Nusselt number will reach a certain value as the convection heat transfer coefficient reaches a constant value. From Table 3-2 it can also be seen that the mesh density is not sufficiently fine enough to give accurate results for case **a** therefore it was necessary to increase the mesh resolution until more acceptable results were achieved.

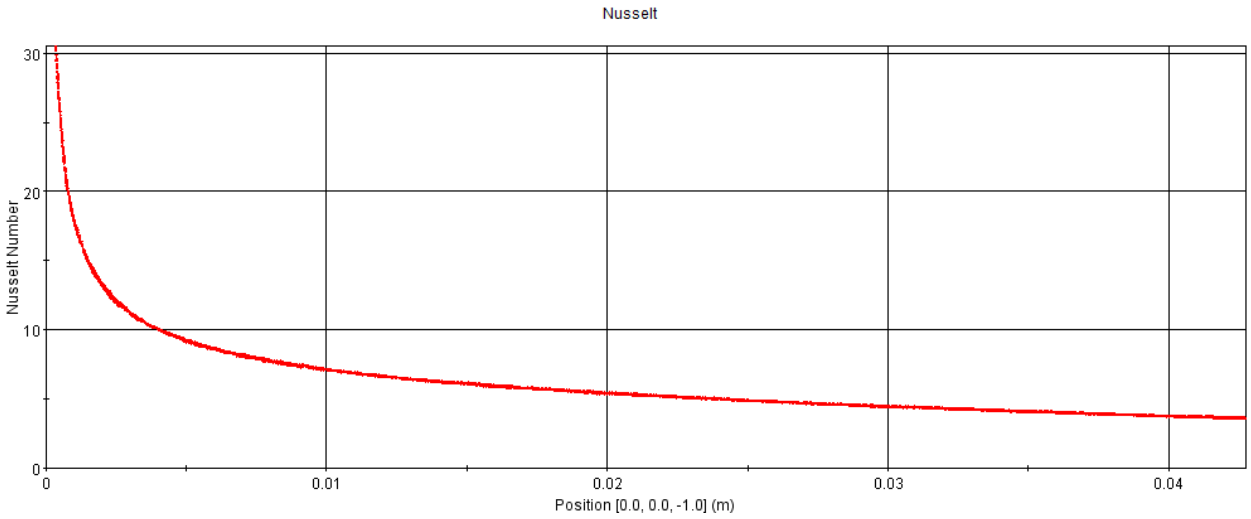

Figure 3-4 - Nusselt number for case b (T)

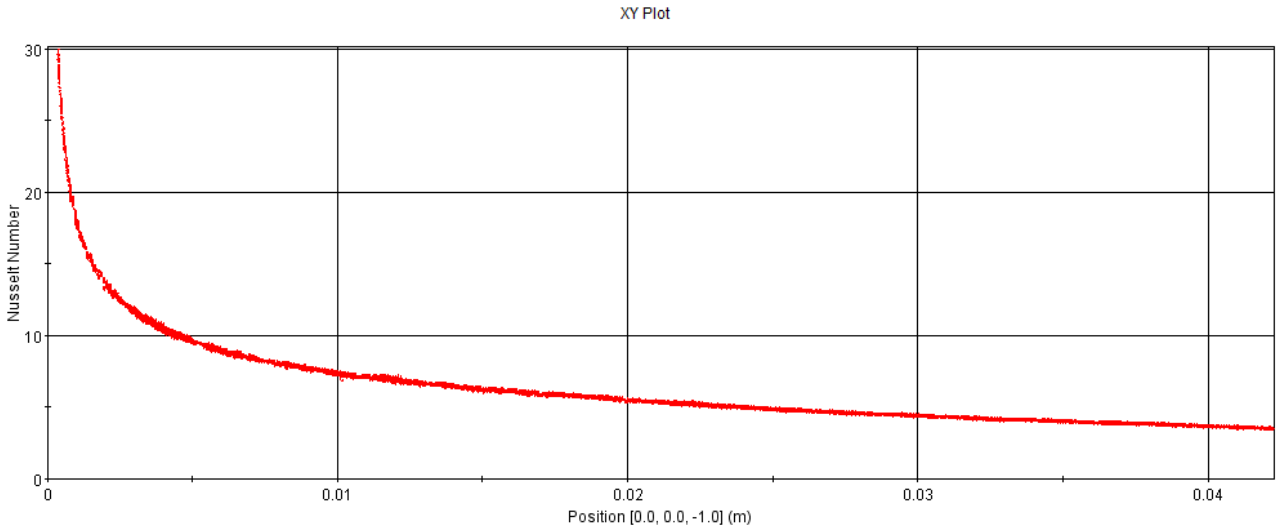

Figure 3-5 - Nusselt number for case c (T)

It can be noted that the Nusselt numbers were extremely large at the entrance of the channel. From equation (2.7) this can be explained as follows:

From the assumption of uniform temperature profile at the inlet equal to T_{wall} the local convection coefficient (h) is very large at the entrance of the tube for all the cases. This is because the thermal boundary layer has a thickness of zero and still needs to be developed (Incropera *et al.*, 2006). As the flow develops the boundary layer grows leading to a decrease in h but stabilizing once the boundary layer is developed.

Figure 3-6 represents the velocity profile within the channel for case **c**. The green profile is located at the entrance of the channel; the red profile midway through the developing region and the blue profile represents fully developed flow at the distance L_t. It can be noted how this resembles Figure 2-13 that is presented from literature. The axial distance from the inlet (for different profiles) will differ from case to case. It can be seen from equations (2.1) and (2.2) that the Reynolds number, Prandtl number and the hydraulic diameter all characterize the development of the profile at a certain distance from the inlet.

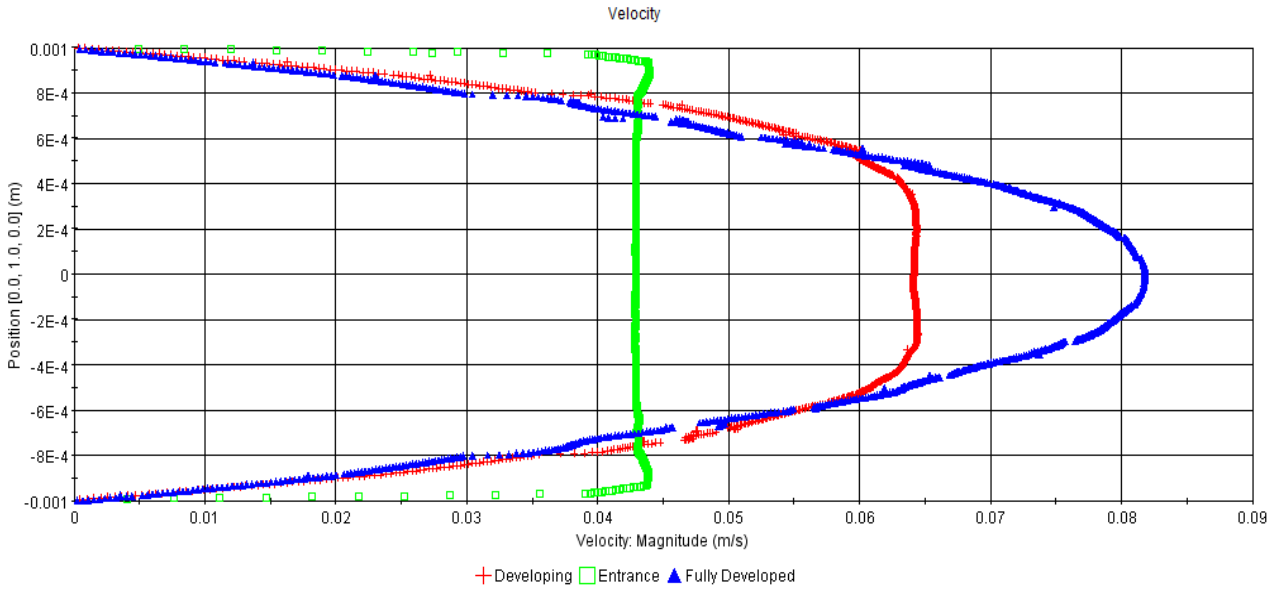

Figure 3-6 - Developing velocity profile

When using equation (2.2) for the fully developed velocity profile and comparing it with Figure 3-6 for the fully developed velocity profile, STAR-CCM+ delivers accurate results. This can be seen in Figure 3-7.

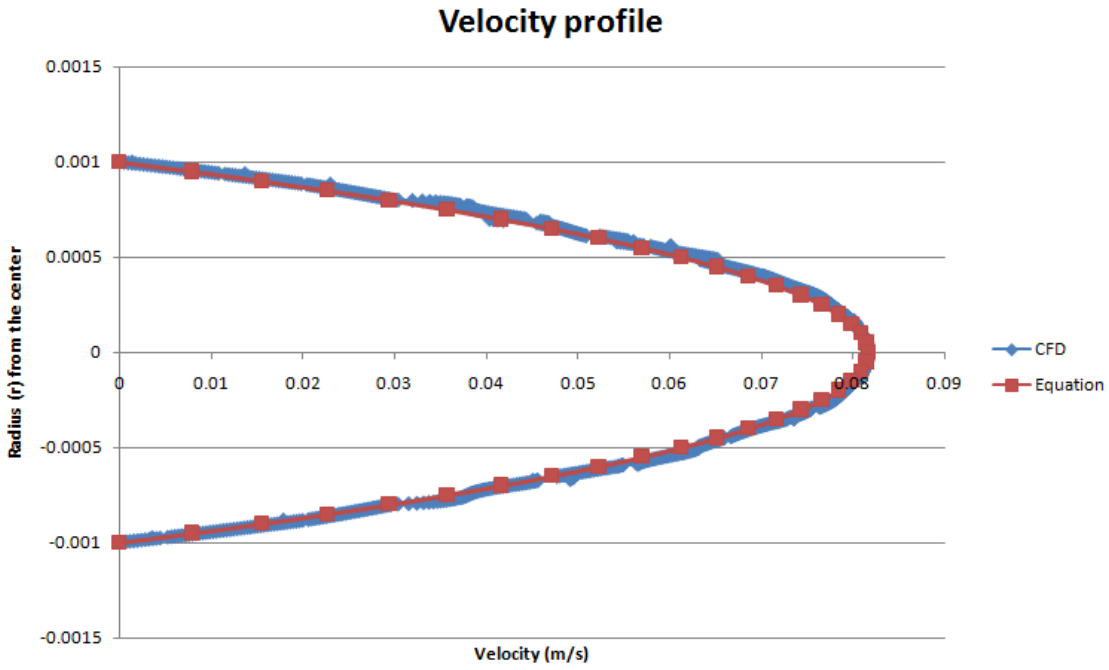

Figure 3-7 – Comparative velocity profiles

It can be seen that accurate results, for the *T* boundary condition, can be provided by STAR-CCM+. The importance of the mesh setup is illustrated through the degree of variation as shown in Table 3-2. It was therefore deemed necessary to do a mesh independency test on the more complicated geometries to ensure that accurate results will still be achieved, with an economic use of resources.

3.3. Comparative *T* boundary condition

In this section a comparison between computational tools will be made. As previously mentioned the extruder tool from STAR-CCM+ can only be used to extend or be added on to an existing volume mesh. In this section a symmetry plane has been used for the *T* boundary condition and the results compared to the results from the previous section. All the properties were kept the same (wall temperature, inlet velocity etc.)

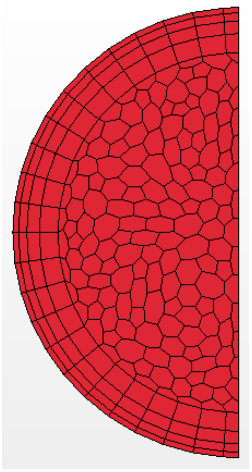

Figure 3-8 - Inlet region mesh (Symmetry case)

Figure 3-8 is an illustration of the inlet region mesh. Comparison between the number of cells used are presented in Table 3-3.

Table 3-3 - Comparative volume cells

	Full computational domain	**Symmetry plane**
Volume cells	643721	321320

Already it can be seen that the number of computational cells were halved resulting in quicker computational time and resources are not wasted.

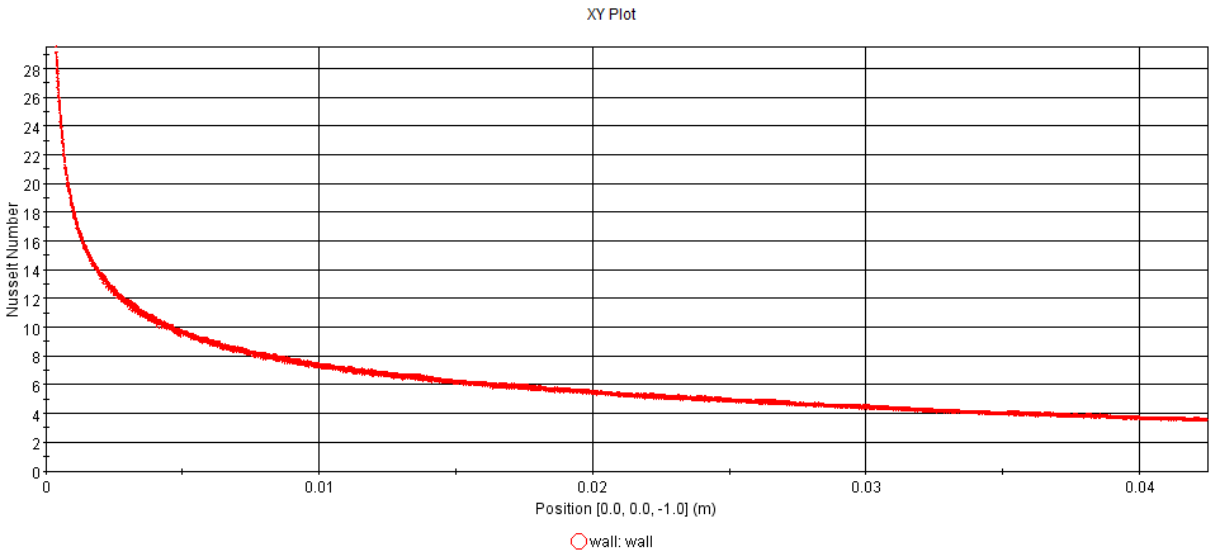

Figure 3-9 - Nusselt number (symmetry plane)

The Nusselt number at L_t is given as 3.6 compared to the 3.69 as with the full computational domain. This results in an error of 1.64% meaning that sufficiently accurate results were still obtained when comparing literature and the numerical results.

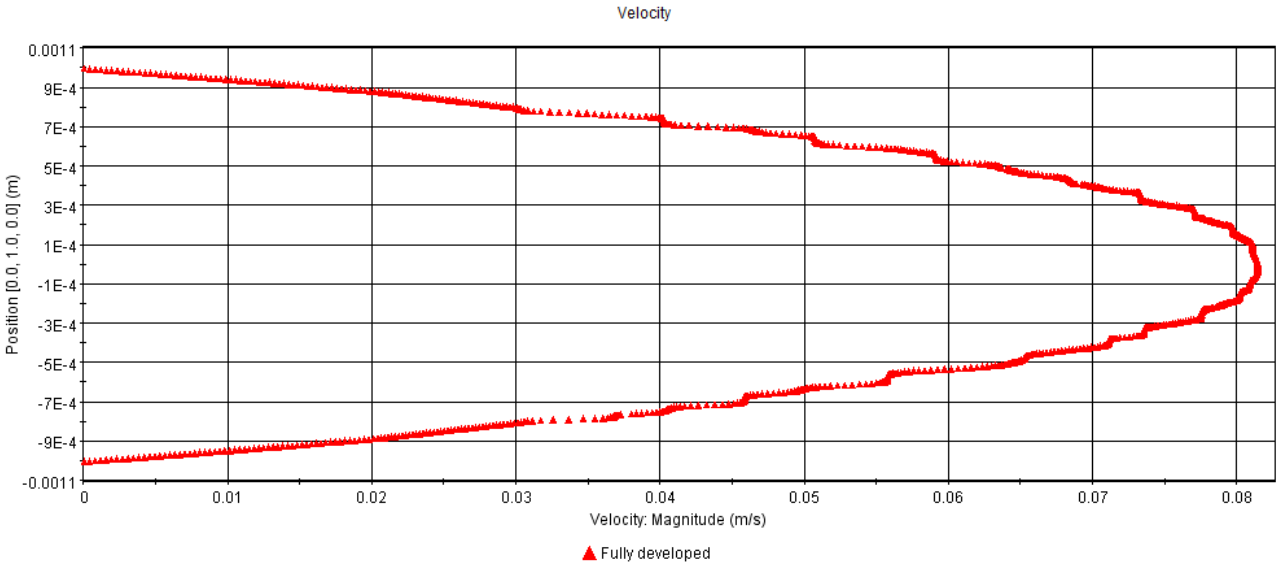

Figure 3-10 - Velocity profile (symmetry plane)

Comparing Figure 3-10 to Figure 3-6 it can be concluded that a good comparison existed between the symmetry plane simulation and the full domain simulation. In conclusion it can be said that there are alternative meshing options that can be considered. It is however dependent on the application, geometry and desires of the user. No further investigation will follow in terms of usable mesh possibilities as these techniques cannot be used for the 3-D channels and solids.

3.4. Mesh independency (H2 boundary condition)

In this section the *H2* boundary will be applied. Once again a mesh independency study was done with the same mesh densities as with the *T* boundary. The same geometry was used so there was no need for different mesh topologies or resolutions to be investigated.

The boundary conditions and fluid properties (steady state) are as follows:

Table 3-4 - H2 boundary (Properties)

Properties	**Value**
Specific heat (C_p)	4183 J/kg-K
Density (ρ)	996.6 kg/m^3
Dynamic viscosity (μ)	0.0008542 kg/m-s
Thermal conductivity (k)	0.6203 W/m-K
Hydraulic diameter (D_h)	2 mm
Length (L)	100 mm
Reynolds number (Re)	100 (-)
Prandtl number (Pr)	5.761 (-)
Inlet velocity	0.04286 m/s
Inlet temperature	300 K
Wall heat flux	1000 W/m^2

The inlet region mesh distributions were exactly the same as shown in Figure 3-2 meaning the same resolutions of volume cells were used for these cases where the only change was the wall boundary condition.

The results were found as follows:

Table 3-5 - H2 boundary (Results)

#	**Base Size**	**Prism Layer Thickness (Fixed at 10% base size)**	**Volume Cells**	**Nusselt (*H2*)**	**Nusselt (L_t)**	**Error**
a	5 mm	0.5 mm	149880	4.36	4.176	4.2%
b	3 mm	0.3 mm	230584	4.36	4.205	3.5%
c	2 mm	0.2 mm	643721	4.36	4.364	0.09%

It can be seen that the results for the 2mm base size correlates well with the value given in the literature.

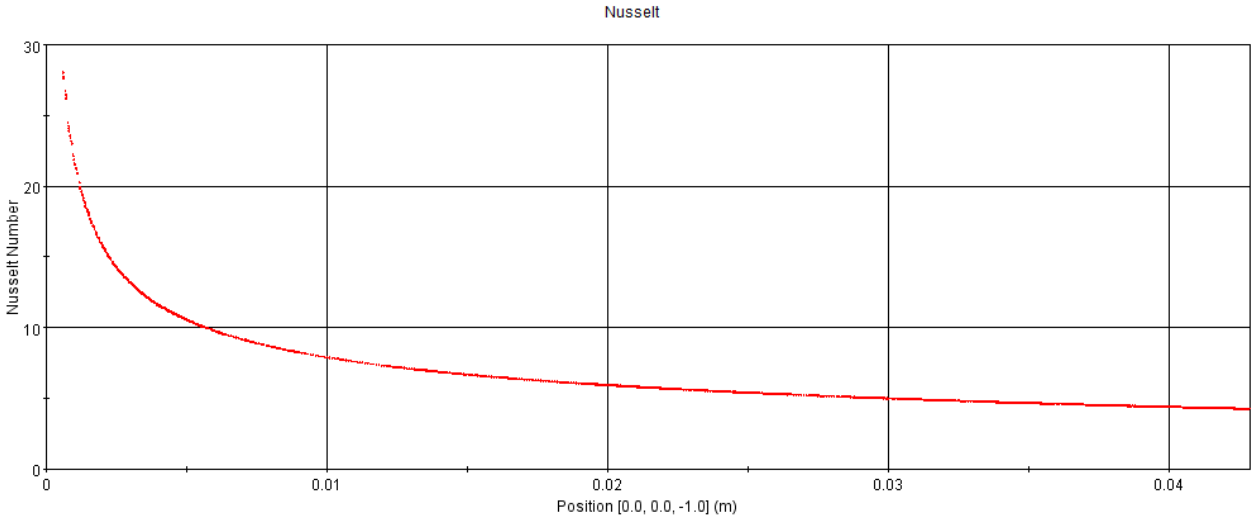

Figure 3-11 - Nusselt number for case a (H2)

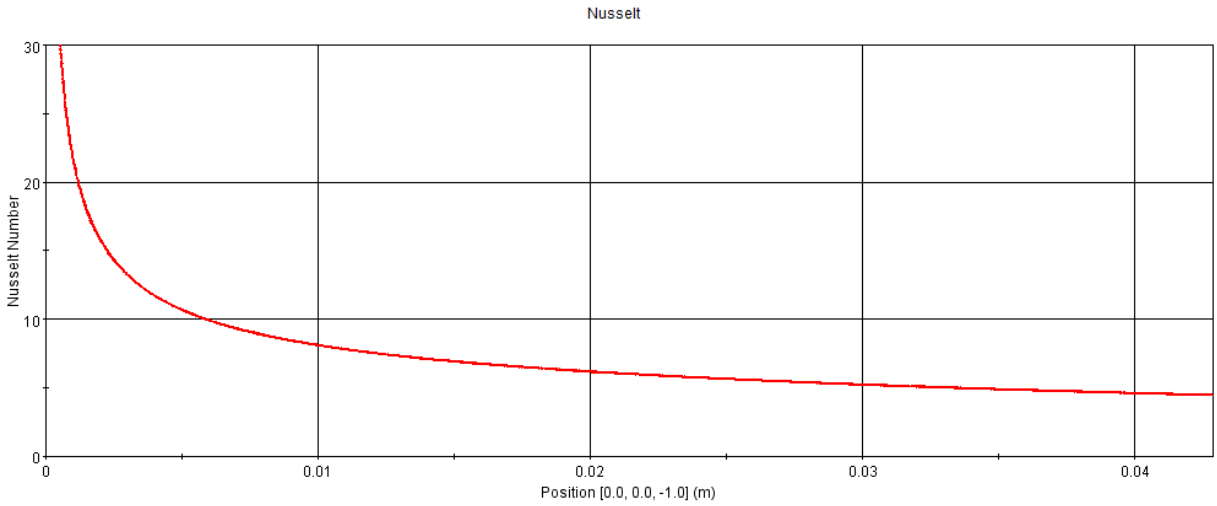

Figure 3-12 - Nusselt number for case b (H2)

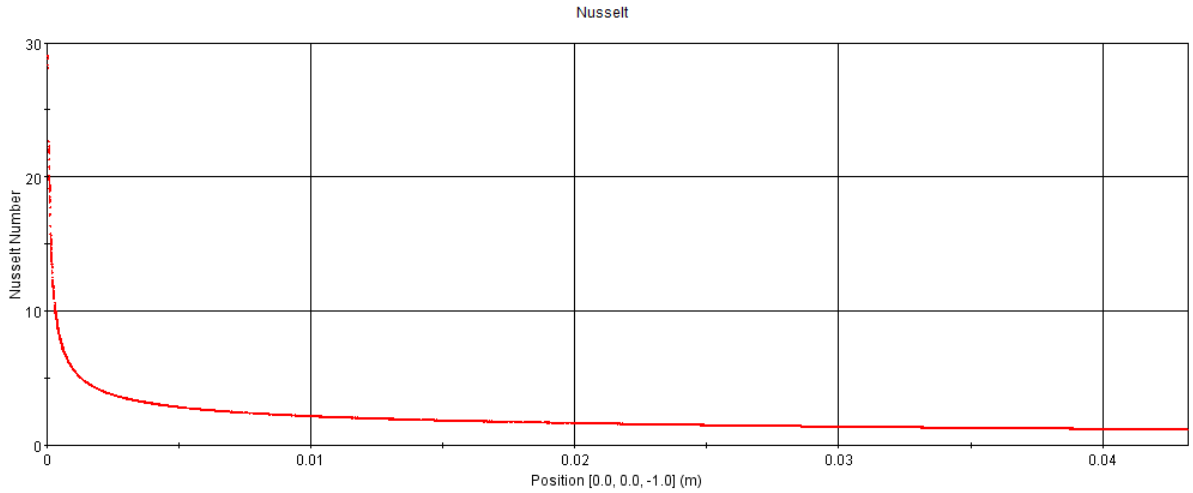

Figure 3-13 - Nusselt number for case c (H2)

Figure 3-11, Figure 3-12 and Figure 3-13 represent the change in the Nusselt number (for the different mesh densities) as a function of the axial distance from the inlet of the channel.

With regards to the *T* and *H2* boundary conditions it can be seen that the simulation methodology applied in STAR-CCM+ provides sufficiently accurate results for the Nusselt number, at the fully developed length, when compared to the results from the literature. The flow within the channel develops as predicted and the associated velocity profile correlates well with the literature when implementing equation (2.2).

In the next section, the validation process with regards to the interface between the fluid and the solid region is described.

3.5. Interface boundary

With the introduction of solid material in the model in this case acting as the confinement of the fluid, there originates the need for a numerical interface between the fluid and the solid regions. The interface acts as the physical and numerical boundary between the two substances across which all of the heat transfer takes place. This is an integrated feature of STAR-CCM+ but it needs to be verified to ensure that the heat transfer between the fluid and the solid is implemented in a correct manner in the test case model.

Two test cases were investigated with regards to the use of the interface boundary:

- Circular channel within a circular solid
- Semi-circular channel within a rectangular solid

In this section the test domains will only be meshed using the polyhedral meshing tool with four prism layers and the optimal grid resolution, as it was determined in the previous section. The specifications include the base size and prism layer size.

The polyhedral meshing tool with the prism layers will be used in the final test cases with multiple channels. For consistency no other mesh tools will thus be investigated for the interface although there were possibilities to decrease the number of computational cells using symmetrical sections. The larger models were also used to stress-test the computer equipment used in terms of total usable mesh sizes.

3.5.1. Circular channel within circular solid

The validation process for this test case was completed as follows. The heat transferred from the solid material to the fluid was determined as well as the heat “received” by the solid from the fluid. These amounts were then compared with each other. It should be noted that the same amount of heat should be transferred in both directions across the interface. The only difference should be the sign from the calculation. Heat should be removed from the solid and added to the fluid according to the problem specification (when heat is removed from the fluid it should thus be the other way round).

Figure 3-14 shows the geometry model that was used in this case. The interface was created between the solid (outer duct) and the fluid (inner duct) using the supplied modelling function in STAR-CCM+.

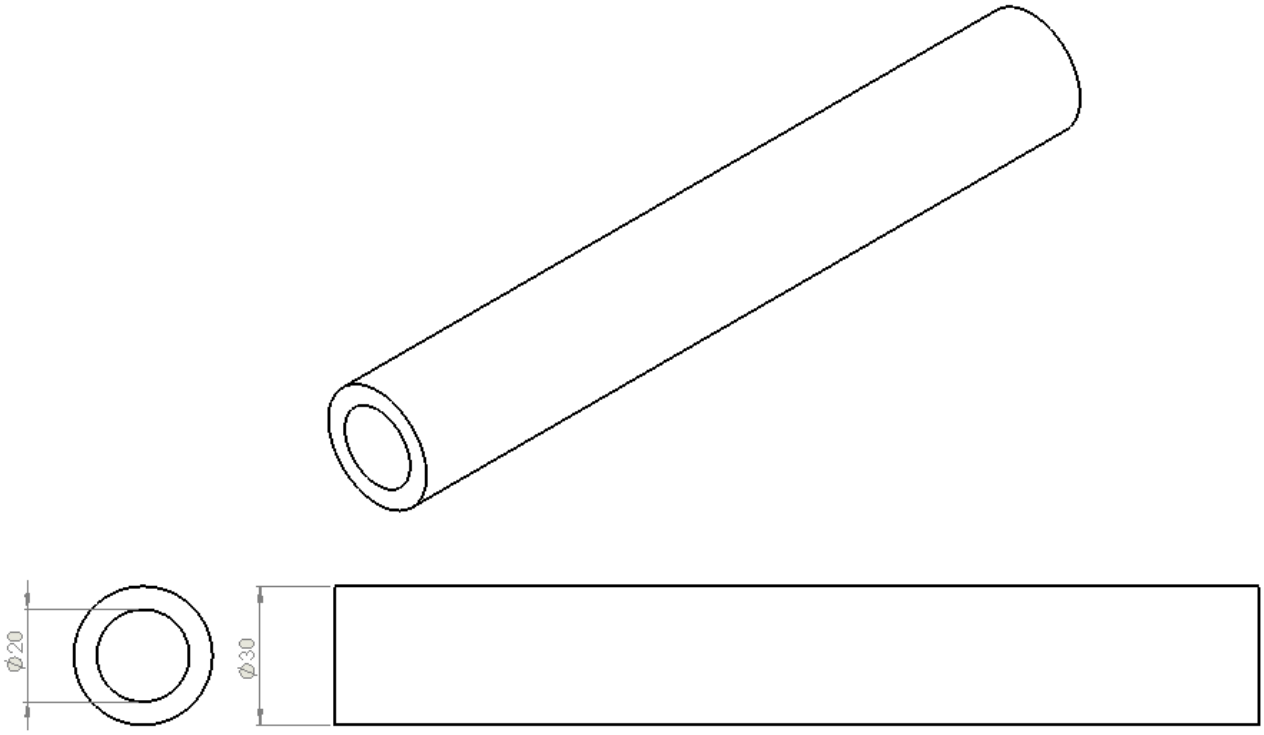

Figure 3-14 - Geometry model (circular, circular)

The geometric details for the model were: a channel diameter of 20 mm, outer diameter of 30 mm and the length of the domain is 200 mm.

The inlet face and boundary mesh distributions are presented in Figure 3-15.

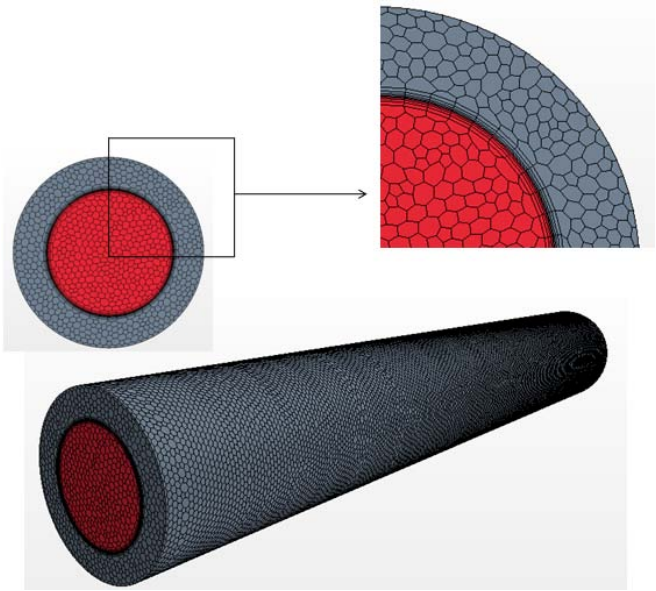

Figure 3-15 - Inlet face and mesh scene (circular, circular)

It consisted of 312584 volume cells with 4 prism layers on each side of the interface (4 on the fluid side and 4 on the solid side) with a total thickness of 2 mm each.

In this case heat was added to the test section from the outer surface of the solid according to the following specifications:

Table 3-6 – Circular duct

Properties (Water)	**Value**	**Properties (Aluminium)**	**Value**
Specific heat (C_p)	4183 J/kg-K	Inner diameter	20 mm
Density (ρ)	996.6 kg/m^3	Outer diameter	30 mm
Dynamic viscosity (μ)	0.0008542 kg/m-s	Wall heat flux	200 W/m^2
Thermal conductivity (k)	0.6203 W/m-K	Initial Temperature	300 K
Hydraulic diameter (D_h)	20 mm	Density (ρ)	2702 kg/m^3
Length (L)	200 mm	Specific heat (C_p)	903 J/kg-K
Reynolds number (Re)	100 (-)	Thermal conductivity (k)	237 W/m-K
Prandtl number (Pr)	5.761 (-)		
Inlet velocity	0.004286 m/s		
Inlet temperature	300 K		

As stated previously the heat transfer over the interface should be of the same magnitude only with a change in the sign as per convention. STAR-CCM+ provides a integrated XY-plot ability. The heat transfer coefficient for the fluid side interface and the solid side interface is plotted as a function of the axial distance from the inlet in Figure 3-16.

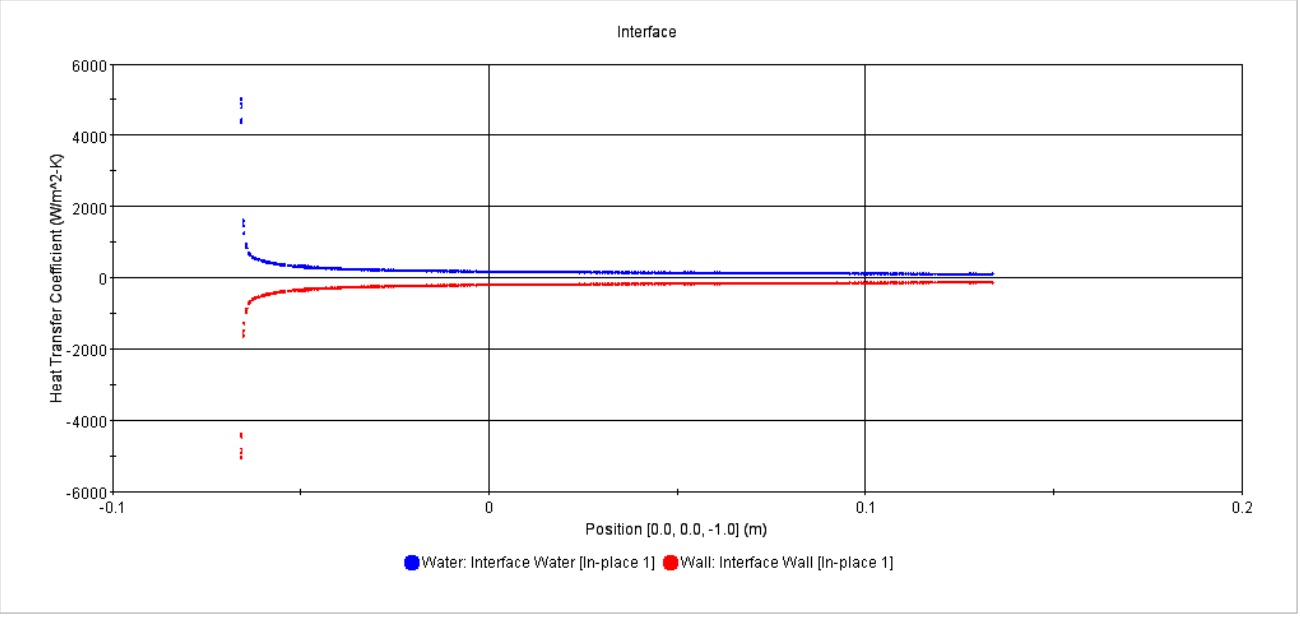

Figure 3-16 - Heat transfer coefficient (circular, circular)

The positive data set represents the localized heat transfer coefficients integrated around the periphery at the fluid side of the interface for different axial locations. The negative data set represents the localized heat transfer coefficients for the solid (Aluminium) side of the interface pair with its associated locations.

Table 3-7 - Heat transfer coefficient ($W/m^2 \cdot K$)

Axial Position From CAD origin	**Heat Transfer Coefficient (Liquid Side)**	**Heat Transfer Coefficient (Solid Side)**
.	.	.
-0.0658	4365.9858	-4365.9858
-0.0658	4454.3125	-4454.3125
-0.0658	4454.4829	-4454.4829
-0.0658	4465.9224	-4465.9224
.	.	.
.	.	.
.	.	.

0.0019	187.0667	-187.0667
0.0018	187.1249	-187.1249
0.0020	183.1516	-183.1516
0.0019	183.7469	-183.7469
.	.	.
.	.	.
.	.	.
0.1051	126.6694	-126.6694
0.1051	124.9919	-124.9919
0.1015	123.4057	-123.4057
0.1021	127.3737	-127.3737

It should be noted, from Table 3-7, that the heat transfer coefficients for both the interfaces (solid and liquid) are the same with only changes in the sign convention. Table 3-7 represents values at certain axial distances from the inlet along the heat transfer interface.

The temperatures through the solid and fluid region at the outlet were theoretically calculated using the following equations:

$$l = \frac{\dot{m}c_p}{\pi D_h q''}(t_{mo} - t_{mi}) \tag{3.1}$$

and

$$t_{so} = \frac{q''}{h} + t_{mo} \tag{3.2}$$

where l is the length of the channel, ṁ is the mass flow rate of the fluid, t_{mo} is the mean outlet temperature of the fluid, t_{mi} is the mean inlet temperature of the fluid and t_{so} is the surface temperature of the solid at the outlet.

The maximum temperature of the solid at the outlet was calculated as 301.9 K. The maximum temperature provided by STAR-CCM+ was 301.83 K. This means that there is only a 0.03% difference between the temperatures. With such a minor difference in the temperatures and looking at the equation (3.2) it can be assumed that the heat transfer over the interface is conserved.

Another feature of symmetrical geometry is that the temperature distribution through the system should be uniform in an azimuthal direction. The next set of figures is located along the axis from the inlet through to the outlet and confirms the uniform distribution for a complete section of the geometry.

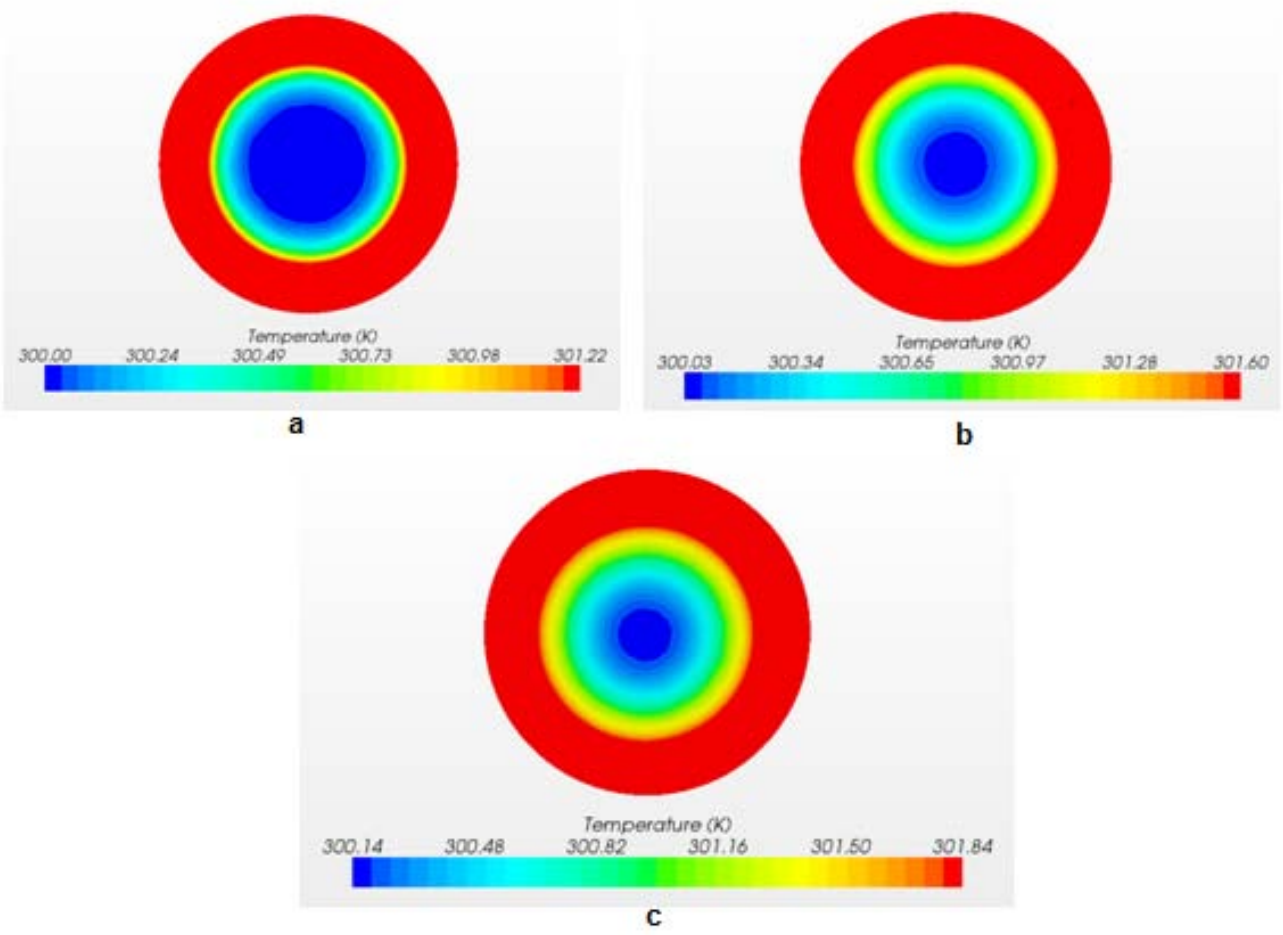

Figure 3-17 - Temperature Distribution
a: inlet b: middle c: outlet

Figure 3-17 illustrates the temperature distribution through the solid and the liquid with Figure 3-17(a) near the inlet, Figure 3-17(b) in the middle of the channel (axially) and Figure 3-17(c) is located at the exit of the channel. It can be seen that when heat was added in a uniform manner the temperature was also distributed symmetrically when the shapes of the fluid and the solid are symmetrical.

3.5.2. Semi-circular channel within rectangular solid

The same modelling approach was used in this case as with the previous case. The changes are that a rectangular geometry was used and that heat was extracted (via the outer surface of the domain) from the fluid and not added to the fluid.

The geometry of the model is illustrated as in Figure 3-18 with the semi-circle having a diameter of 2 mm and the rectangle is 4 mm in width and 3 mm in height.

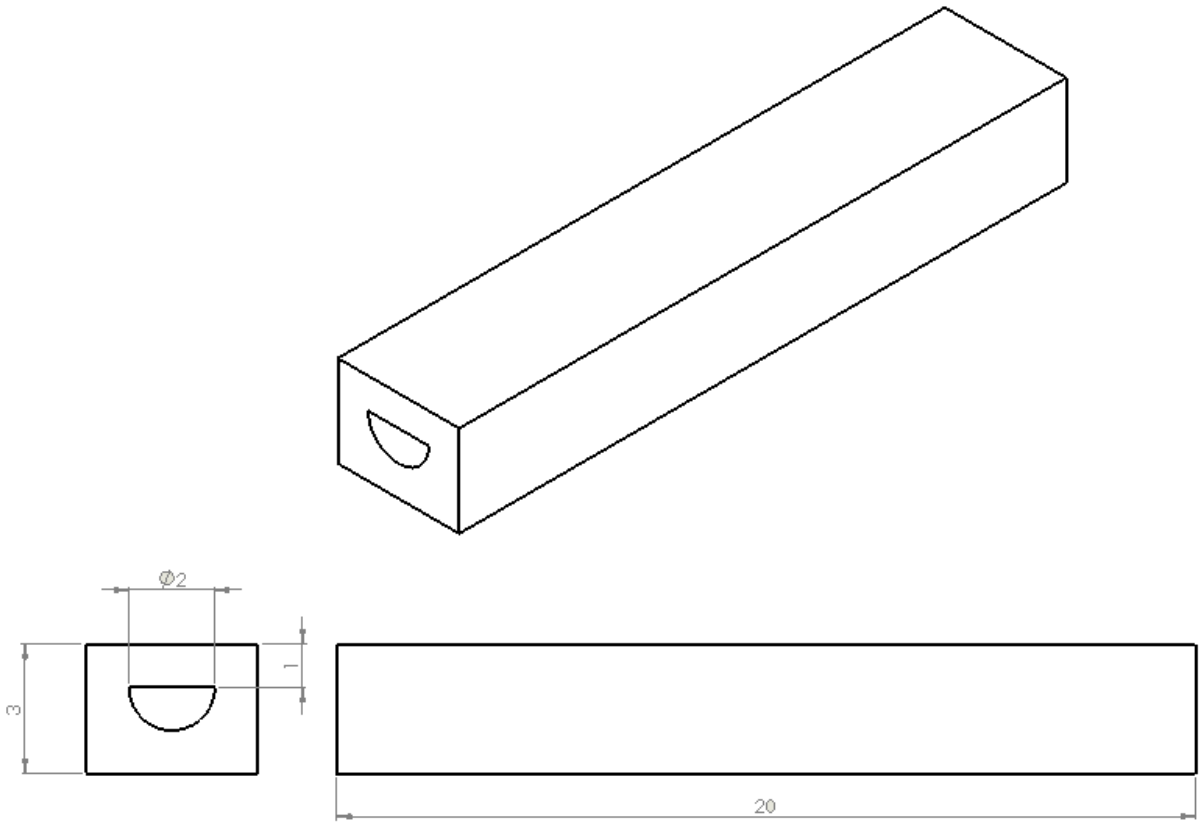

Figure 3-18 – Semi-circular channel in rectangular domain

The model was meshed using the STAR-CCM+ integrated polyhedral and prism layer meshing tools. The model consisted of 112838 volume cells, 4 prism layers for both the solid and the fluid sides of the interface with a total layer thickness of 0.2 mm measured from the interface inwards to the fluid and outwards from the interface into the solid.

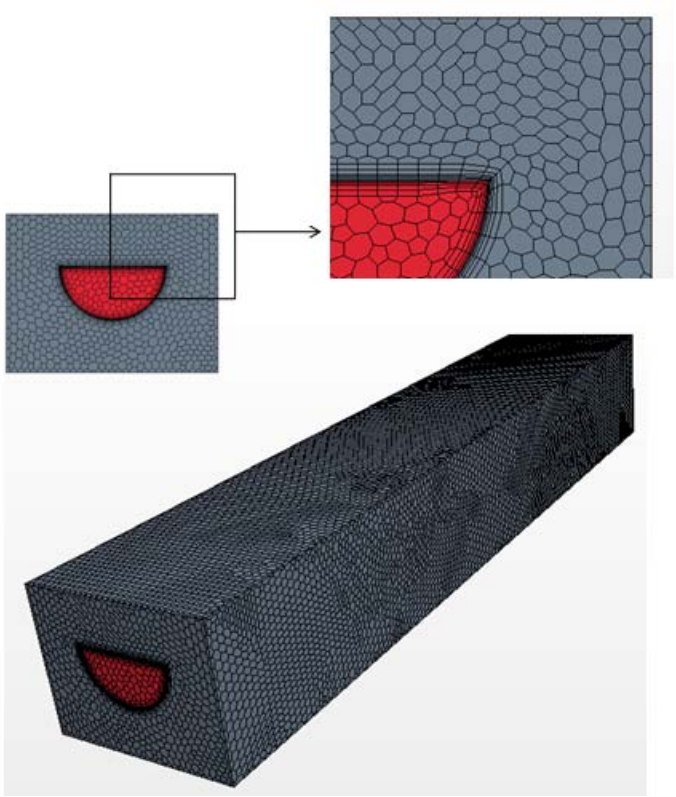

Figure 3-19 - Inlet face and mesh scene (semi-circle, rectangle)

Figure 3-19 illustrates the mesh configuration used in the simulation with properties as tabulated in Table 3-8.

Table 3-8 - Semi-circular duct

Properties (Water)	**Value**	**Properties (Aluminium)**	**Value**
Specific heat (C_p)	4183 J/kg-K	Width	4 mm
Density (ρ)	996.6 kg/m^3	Height	3 mm
Dynamic viscosity (μ)	0.0008542 kg/m-s	Wall heat flux	-5000 W/m^2
Thermal conductivity (k)	0.6203 W/m-K	Initial Temperature	300 K
Hydraulic diameter (D_h)	1.22 mm	Density (ρ)	2702 kg/m^3

Length (L)	100 mm	Specific heat (C_p)	903 J/kg-K
Reynolds number (Re)	100 (-)	Thermal conductivity (k)	237 W/m-K
Prandtl number (Pr)	5.761 (-)		
Inlet velocity	0.07014 m/s		
Inlet temperature	300 K		

As with the previous study the heat transfer coefficient was plotted as a function of the axial distance from the inlet to determine if the heat being transferred was conserved.

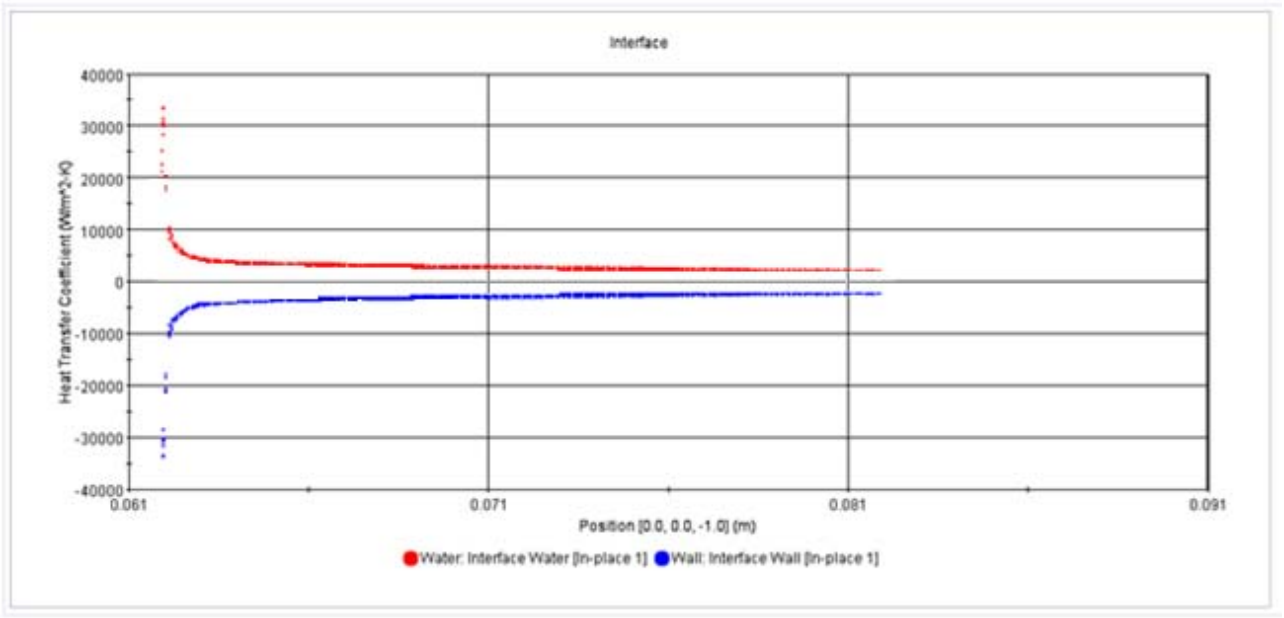

Figure 3-20 - Heat transfer coefficient (semi-circle, rectangle)

It can be noted from Figure 3-20 (and Table 3-9) that the heat transfer coefficient for the corresponding CV with regards to the solid interface side and the fluid interface side is a mirror image about the 0 value axis for the heat transfer coefficient.

Table 3-9 - Heat transfer coefficient (W/m^2·K)

Axial Position From CAD origin	Heat Transfer Coefficient (Liquid Side)	Heat Transfer Coefficient (Solid Side)
.	.	.
0.061946	-30724.9	30724.93
0.061947	-30572.1	30572.08
0.061947	-30502.3	30502.33
0.061947	-30265.9	30265.93
.	.	.
.	.	.
.	.	.
0.075854	-2001.06	2001.058
0.075768	-1894.56	1894.558
0.075848	-1824.51	1824.514
0.075803	-2210.59	2210.589
.	.	.
.	.	.
.	.	.
0.08101	-1914.46	1914.456
0.081166	-1825.51	1825.514
0.081393	-1677.37	1677.368
0.081478	-1636.62	1636.617

The minimum temperature on the surface at the outlet was calculated using equations (3.1) and (3.2) as 293.1 K. The temperature provided by STAR-CCM+ was given as 294.3 K. This resulted in a temperature difference of 0.5%. It is reasonable to assume that the heat transferred across the interface was conserved which means that all the heat extracted from one side of the interface was added to the other side.

As noted in the previous case where the temperature distribution was uniform in an azimuthally direction, in this study it will not be the case. The heat is not extracted evenly from the fluid so the temperature will also not be symmetrically distributed in the azimuthally direction throughout the solid.

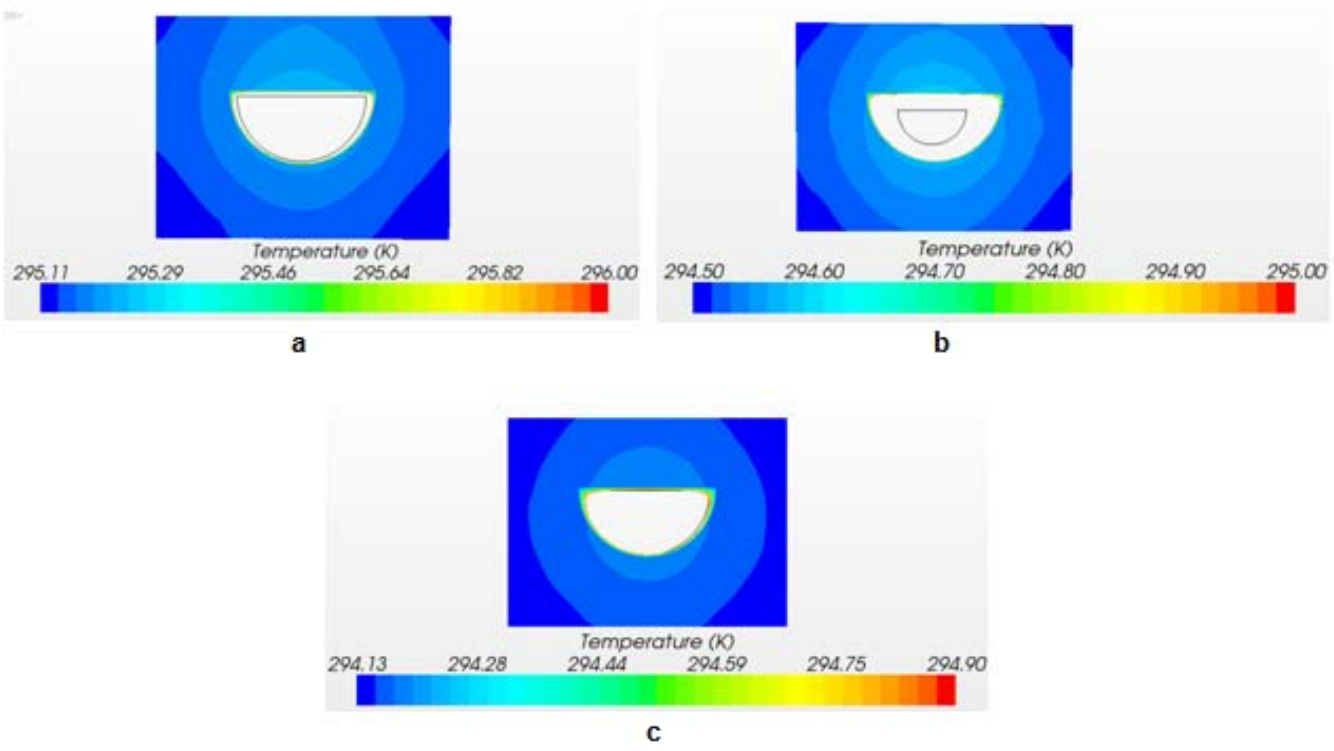

Figure 3-21 - Temperature distribution (semi-circle, rectangle)

Figure 3-21 illustrates the temperature distribution through the solid with Figure 3-21(a) near the inlet, Figure 3-21(b) in the middle of the channel (axially) and Figure 3-21(c) is located at the exit of the channel. The temperature plots have been bounded, as indicated, to better show the temperature distribution through the solid. The temperature of the fluid is not shown, thus the white space in the middle of the figure. It can be seen that the temperature is not distributed symmetrically around the circumference through the solid.

3.6. Conclusion

It should be noted that the meshing tools (tetrahedral, trimmer and extruder) were not used during all the validation cases. Although more computational resources were utilized in some of the validation cases than optimally required, it was done to maintain computational workload consistency between validation cases and final investigative models. The final test cases will be based (mesh setup) on the conclusions from this chapter.

From the validation results it was clear that the software delivered sufficiently accurate results in terms of the Nusselt number and how the velocity profile develops through the channel. The test cases were solved to accuracy within 1% of the values obtained from the literature with regards to the Nusselt number. The heat transfer over the interface was conserved. The heat transferred coefficient over the interface was equal for heat addition and removal as seen in Table 3-7 and Table 3-9. This indicates that the solvers and mesh setups used were correctly implemented in the model to solve and deliver accurate results when compared to the literature and analytical calculations.

4 Design evaluation and methodology

In this chapter the focus is on the description of new factors which were used to evaluate the test cases described in the following chapter. Detailed descriptions of these factors and the methodology used will follow later in this chapter.

4.1. Design evaluation

In this section the focus is on the quantification of the factors that were used to evaluate the different conceptual layouts investigated in the study.

4.1.1. The volume ratio

The volume ratio factor gives the ratio of the fluid to solid volume and is defined as:

$$V_r = \frac{V_c}{V_s} \tag{4.1}$$

where V_c is the volume of the channel and V_s is the volume of the solid in a certain control volume which consists of the whole volume (including the volume of the channel).

The volume ratio also gives an indication of the stacking ability of the layout that was used. The larger the value of the ratio, the better the stacking ability of the layout and ultimately more effective the use of the surrounding material. It is also an indication of effective material usage as a larger volume ratio implies larger area density (heat exchange area is larger). This means that the material is used more effectively in heat transfer.

The 3 layouts that were used in this study are represented by Figure 2-6, Figure 2-7 and Figure 2-8 in the literature survey chapter.

The dashed lines in Figure 4-1 represent the area (for a serpentine shape) used to calculate the volume for the solid surrounding the fluid for one periodic section of the layout. The area was multiplied by the thickness of the plate to estimate the volume.

The dashed lines in Figure 4-2 represents the area for a trapezoidal shape that was used to calculate the volume of the solid surrounding the fluid. It can be noted visually that the ratio for a trapezoidal shape should be higher than that of the serpentine shape.

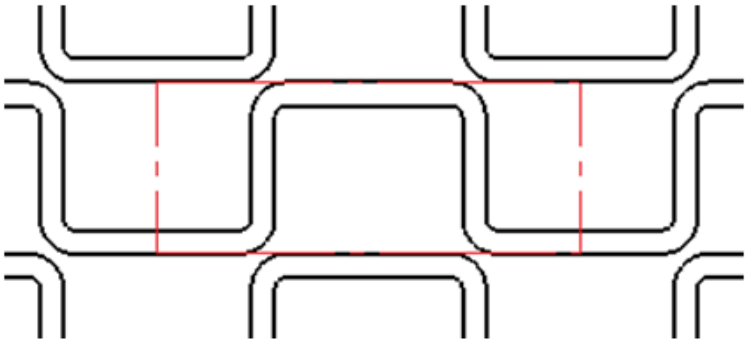

Figure 4-1 - Control volume for serpentine layout

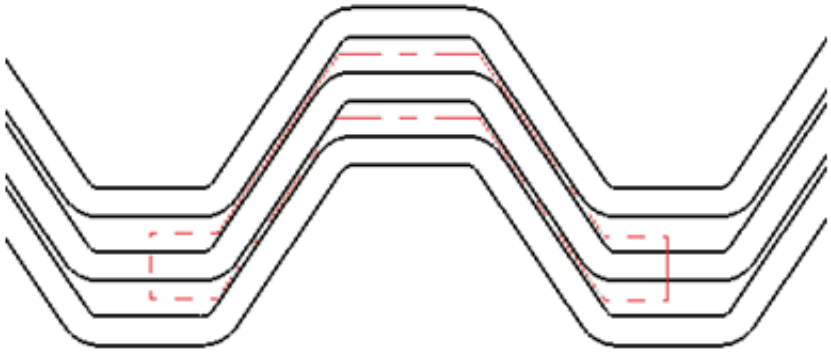

Figure 4-2 - Control volume for trapezoidal shape

The dashed lines in Figure 4-3 represents the area used for a zigzag shaped layout. In all 3 cases the plate areas were multiplied by the thickness of a single plate (for each test case) to determine the volume of the surrounding material.

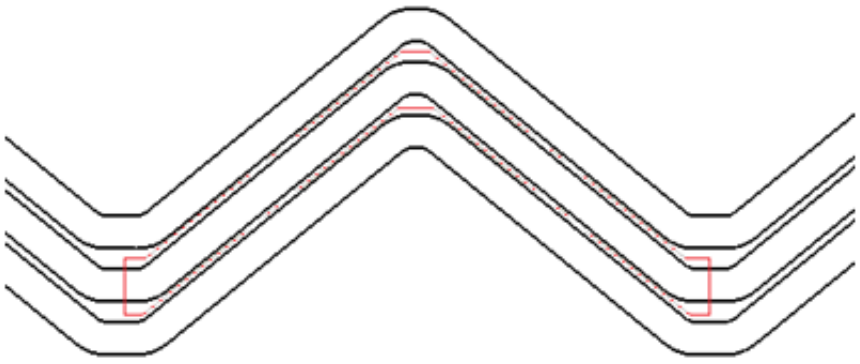

Figure 4-3 - Control volume for zigzag shape

The volumes of the channels were computed by multiplying the flow cross-section area of the channel with the pathway length of one period for the layout.

4.1.2. The “heat spots”

Heat spots can be classified as an area with a clearly discernable boundary in the solid region that is at a significantly different temperature, whether higher or lower (depending on which plate, secondary or primary is being simulated) than the fluid in the channels.

The heat spots could be found by visual inspection between the channels and the analysis of the heat spots are shown in the next chapter. These heat spots will dominate in layouts where channels do not stack well with each other. This is usually found when there is a relatively large solid area between adjacent channels, as in the case of serpentine channel layouts.

Heat spots therefore also give an indication of how effective the materials are being used and the thermal inertia of solid material in a specific heat exchanger design. The size of the heat spots quantifies the effective use of the surrounding material where larger temperature differences between the fluid and solid indicates lesser amounts of heat transferred immediately between fluid streams.

4.1.3. Temperature difference

The temperature difference plots the temperature of the surrounding solid relative to the temperature of the fluid. These sets of values are plotted from a line probe as indicated in Figure 4-4.

Figure 4-4 - Temperature difference line probe

The line probe was located in between the neighbouring micro-channels (through the solid and the fluid) and measures only the middle micro-channel fluid temperature. It was also located axially from the inlet of the channels at the point were fully developed flow has been reached. It is measured at the same point for each of the test cases. The values obtained were averaged and subtracted (solid from the fluid) to give the temperature difference between the fluid and the solid region.

4.1.4. Enhancement factor

The enhancement factor can be used as an indication of how much a layout enhances or improves the effectiveness of material usage. This is measured according to a relation of volume ratio to the temperature difference and is given as:

$$E_f = \frac{Volume\ ratio}{Temperature\ difference} \tag{4.2}$$

From equation (4.2) it can be seen that a bigger volume ratio and smaller temperature difference will result in a larger enhancement factor. A larger enhancement factor implies more effective material usage for immediate heat transfer, while a smaller factor indicates higher thermal storage in the exchanger material itself.

4.2. Methodology

The methodology used for each test case was as follows:

Table 4-1 - Mesh configuration

Base Size	Number of prism layers	Total prism layer thickness (percentage of base)
2 mm	4	10

Table 4-1 tabulates the mesh configuration used for each setup. The integrated polyhedral mesh and prism layer tool from STAR-CCM+ was used to construct the meshes. After the volume mesh was generated another integrated tool of STAR-CCM+ was used to determine the number of bad cells. These cells were then repaired using the integrated mesh repair tool.

The interfaces between the solid and the fluid is a contact-interface which was defined using the standard feature of Star-CCM+.

The inlets of the channels were specified as velocity inlet types. The velocities for the inlets were calculated using equation (2.4). The outlets of the channels were specified as pressure outlet types. The outlet pressures were specified with atmospheric pressure as reference.

The outer boundaries of the domain were specified as plane walls. Although there exist hundreds of periodical channels in a heat exchanger, simulations were restricted to only three channels. The boundary walls, as mentioned, were specified as plane walls and only the middle channel was evaluated. It was assumed that the a fourth or fifth channel would not have a significant effect on the centre channel. Only three channels were “stacked” on a plate to minimize the number of volume cells used.

The heat flux (positive or negative, depending whether a primary or secondary plate layer was simulated) was applied to the top and bottom planes. From Figure 5.1 it can be noted that heat could be added or extracted from the top and bottom plates. The magnitudes of the heat fluxes for each case are presented in Table 5-2, Table 5-3, and Table 5-4.

The solver settings used were the segregated fluid and segregated energy solver options.

5 Test cases and results

In this chapter the results from test cases investigated in this study are presented. The volume ratio, occurrence of heat spots and temperature distribution for each case are presented. In these models multiple channels (3) were “stacked” alongside each other in the plate. The configurations of the models are presented in Figure 5-1.

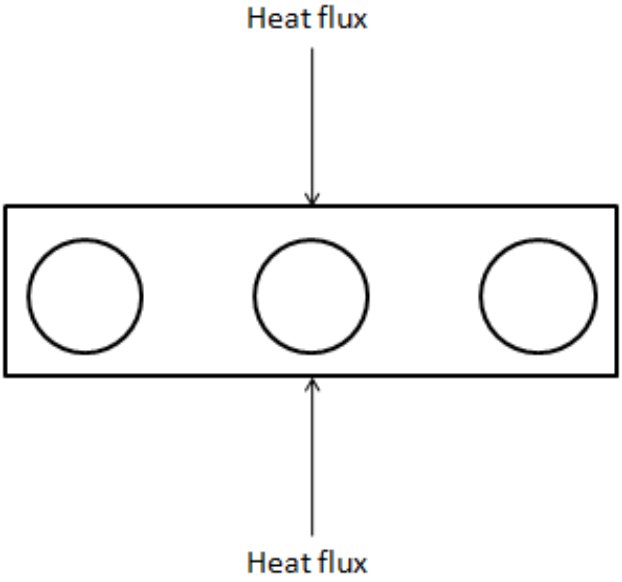

Figure 5-1 - Simulation configuration showing top and bottom of typical test section with boundaries

Figure 5-1 represents a simple front view of the basic layout for the test cases to follow. It should be noted that heat fluxes were applied to both the upper and the lower plane of the configuration. In the introduction it was explained that secondary plates are on both sides of the primary plates, whether using a hot or cold fluid. This is why heat fluxes are applied on the top and bottom plane. More detailed descriptions of each case are presented separately.

The order of the geometrical layouts as presented in this chapter is the serpentine layout, trapezoidal layout and then the zigzag layout.

5.1. Configurations

This section will give a summary of the simulation properties and the configurations of the various layouts. The geometric ratios of the configurations are presented in Table 5-1.

Table 5-1 - Ratios for layouts

Ratio	Serpentine	Trapezoidal	Zigzag
R_c/d	1	1	1
L/d	9	9	9
B/L	1	0.55	0.1
A/L	0.7	0.7	0.7

The dimensions of the layouts were determined from the non-dimensional ratios stated in Table 5-1 based on a channel diameter of 2mm. When these ratios are applied, the dimensions for each parameter as seen in Figure 2-5, are determined and the channels designed accordingly.

5.1.1. Serpentine configuration

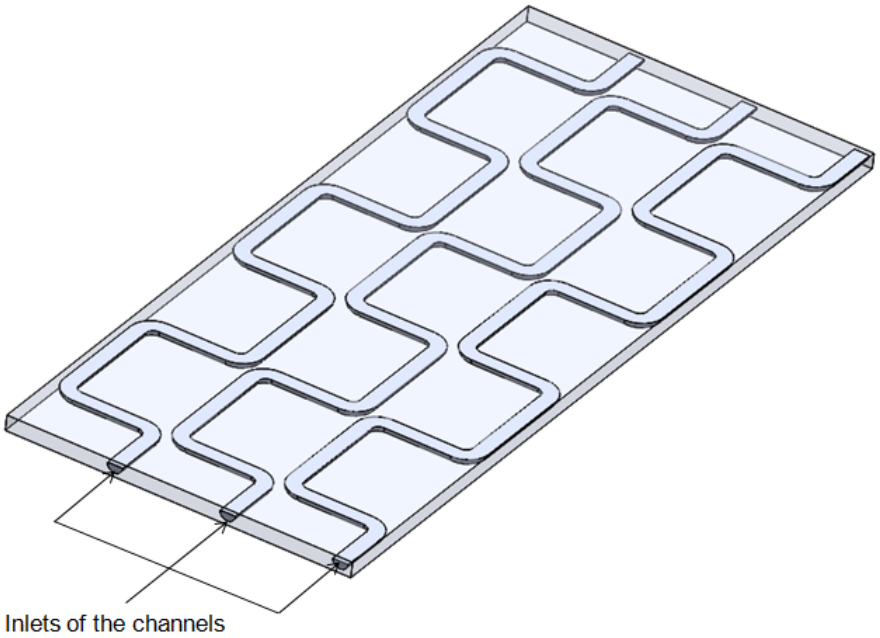

Figure 5-2 - Serpentine layout

Figure 5-2 represents the layout of the serpentine setup. The solid material surrounding the channels is represented by the transparent rectangle enclosing the fluid channels. The inlets (semi-

circles) were specified as velocity inlets, the outlets as pressure outlets, the interfaces between fluid and solid as contact interfaces, and the remainder of the walls as adiabatic boundaries.

The parameters of the simulation are presented in Table 5-2.

Table 5-2 - Simulation parameters for serpentine layout

Properties (Water)	**Value**	**Properties (Aluminium)**	**Value**
Specific heat (C_p)	4183 J/kg-K	Width	44.8 mm
Density (ρ)	996.6 kg/m^3	Length	108 mm
Dynamic viscosity (μ)	0.0008542 kg/m-s	Thickness	2 mm
Thermal conductivity (k)	0.6203 W/m-K	Heat flux (per plane)	10439 W/m^2
Diameter of semi-circle (d)	2 mm	Initial Temperature	300 K
Hydraulic diameter (D_h)	1.222 mm	Density (ρ)	2702 kg/m^3
Length per period (L)	57.77 mm	Specific heat (C_p)	903 J/kg-K
Reynolds number (Re)	1000 (-)	Thermal conductivity (k)	237 W/m-K
Prandtl number (Pr)	5.761 (-)		
Inlet velocity (for each channel)	0.7284 m/s		
Inlet temperature	300 K		

A partial inlet region mesh is presented by Figure 5-3.

Figure 5-3 – Partial inlet region mesh for serpentine layout

In Table 4-1 the mesh configurations for all the test cases are presented. The serpentine layout consisted of 1282179 volume cells in total.

5.1.2. Trapezoidal configuration

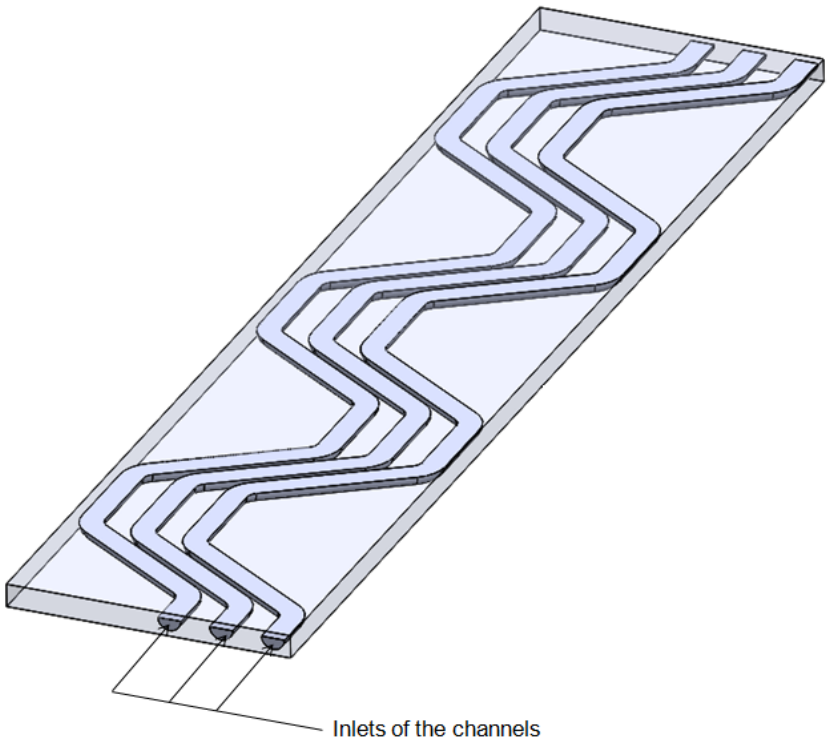

Figure 5-4 - Trapezoidal layout

The layout for a trapezoidal configuration is presented in Figure 5-4. It can be noted visually that it already “stacks” better than channels of a serpentine geometry. The problem parameters and boundary conditions for this layout are the same as for that of the serpentine layout. The shape of the layout differs together with the size of the surrounding solid. The sizes of the solid regions

between channels already give an indication of the stacking ability for trapezoidal channels versus serpentine channels.

The parameters for the trapezoidal models are presented in Table 5-3.

Table 5-3 - Simulation parameters for trapezoidal layout

Properties (Water)	**Value**	**Properties (Aluminium)**	**Value**
Specific heat (C_p)	4183 J/kg-K	Width	24.58 mm
Density (ρ)	996.6 kg/m^3	Length	108 mm
Dynamic viscosity (μ)	0.0008542 kg/m-s	Thickness	2 mm
Thermal conductivity (k)	0.6203 W/m-K	Heat flux (per plane)	18832 W/m^2
Diameter of semi-circle (d)	2 mm	Initial Temperature	300 K
Hydraulic diameter (D_h)	1.222 mm	Density (ρ)	2702 kg/m^3
Length per period (L)	48.73 mm	Specific heat (C_p)	903 J/kg-K
Reynolds number (Re)	1000 (-)	Thermal conductivity (k)	237 W/m-K
Prandtl number (Pr)	5.761 (-)		
Inlet velocity (for each channel)	0.7284 m/s		
Inlet temperature	300 K		

It can be noted that the applied heat flux differed between the trapezoidal and a serpentine layouts. To compare the layouts they were all simulated under the same conditions. It was determined that the energy added to the test section should be 100 Watts. With a smaller plate area in the test

section for the trapezoidal and zigzag case, the heat flux applied had to be larger to ensure that an equal amount of Watts were added to the domain.

Figure 5-5 represents a partial inlet region mesh for the trapezoidal layout and consisted of 1371132 volume cells in total.

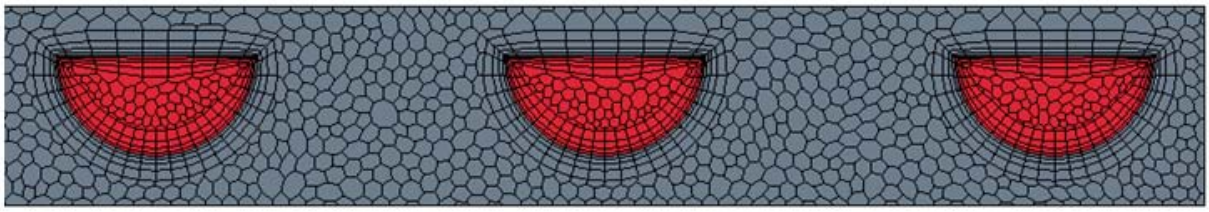

Figure 5-5 – Partial inlet region mesh for trapezoidal layout

5.1.3. Zigzag configuration

The last configuration that was considered in this study was a zigzag layout. The layout for this configuration is presented in Figure 5-6.

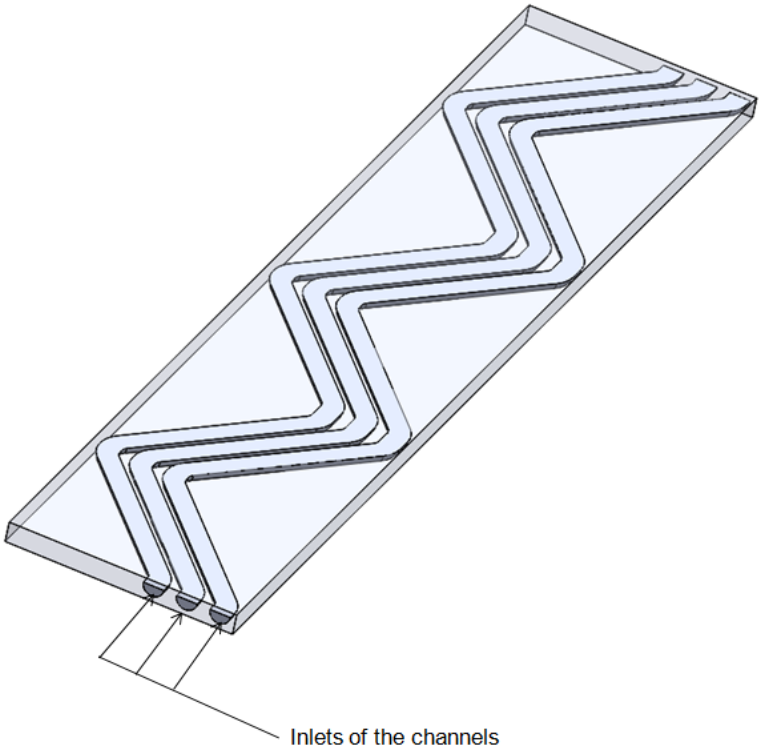

Figure 5-6 - Zigzag layout

The simulation parameters for the zigzag test case are presented in Table 5-4.

Table 5-4 - Simulation parameters for zigzag layout

Properties (Water)	**Value**	**Properties (Aluminium)**	**Value**
Specific heat (C_p)	4183 J/kg-K	Width	22.06 mm
Density (ρ)	996.6 kg/m^3	Length	108 mm
Dynamic viscosity (μ)	0.0008542 kg/m-s	Thickness	2 mm
Thermal conductivity (k)	0.6203 W/m-K	Heat flux (per plane)	20986.5 W/m^2
Diameter of semi-circle (d)	2 mm	Initial Temperature	300 K
Hydraulic diameter (D_h)	1.222 mm	Density (ρ)	2702 kg/m^3
Length per period (L)	44.73 mm	Specific heat (C_p)	903 J/kg-K
Reynolds number (Re)	1000 (-)	Thermal conductivity (k)	237 W/m-K
Prandtl number (Pr)	5.761 (-)		
Inlet velocity (for each channel)	0.7284 m/s		
Inlet temperature	300 K		

In Table 5-4 the difference in the added heat flux can be seen. Considering the three different configurations, from inspection it could be said that the zigzag layout stacks the best.

A partial inlet region mesh is presented in Figure 5-7 for the zigzag layout and it consisted of 1433488 volume cells in total.

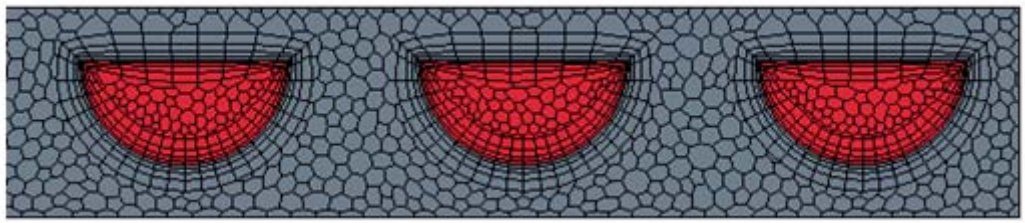

Figure 5-7 –Partial inlet region mesh for zigzag layout

5.2. Results and discussions

In this section the results from the various layouts will be presented and discussed in terms of the temperature distribution (heat spots), the volume ratios and the enhancement factor for the various layouts.

5.2.1. Temperature distribution

Figure 5-8 represents a front view of the section, indicating the location for an inserted plane on which the temperature distribution for the section was plotted.

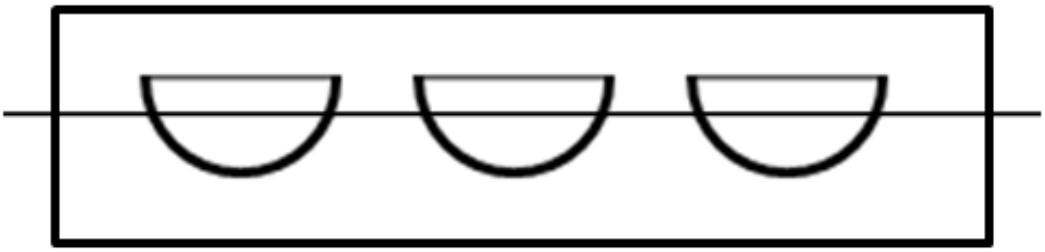

Figure 5-8 - Temperature plane cutting along length of the test section

The next three sets of figures show:

a) The temperature distribution inside the channels alone.

b) Planar plot of the temperature distributions within the solid and the fluid materials.

c) Temperature distribution on the upper surface of the domain.

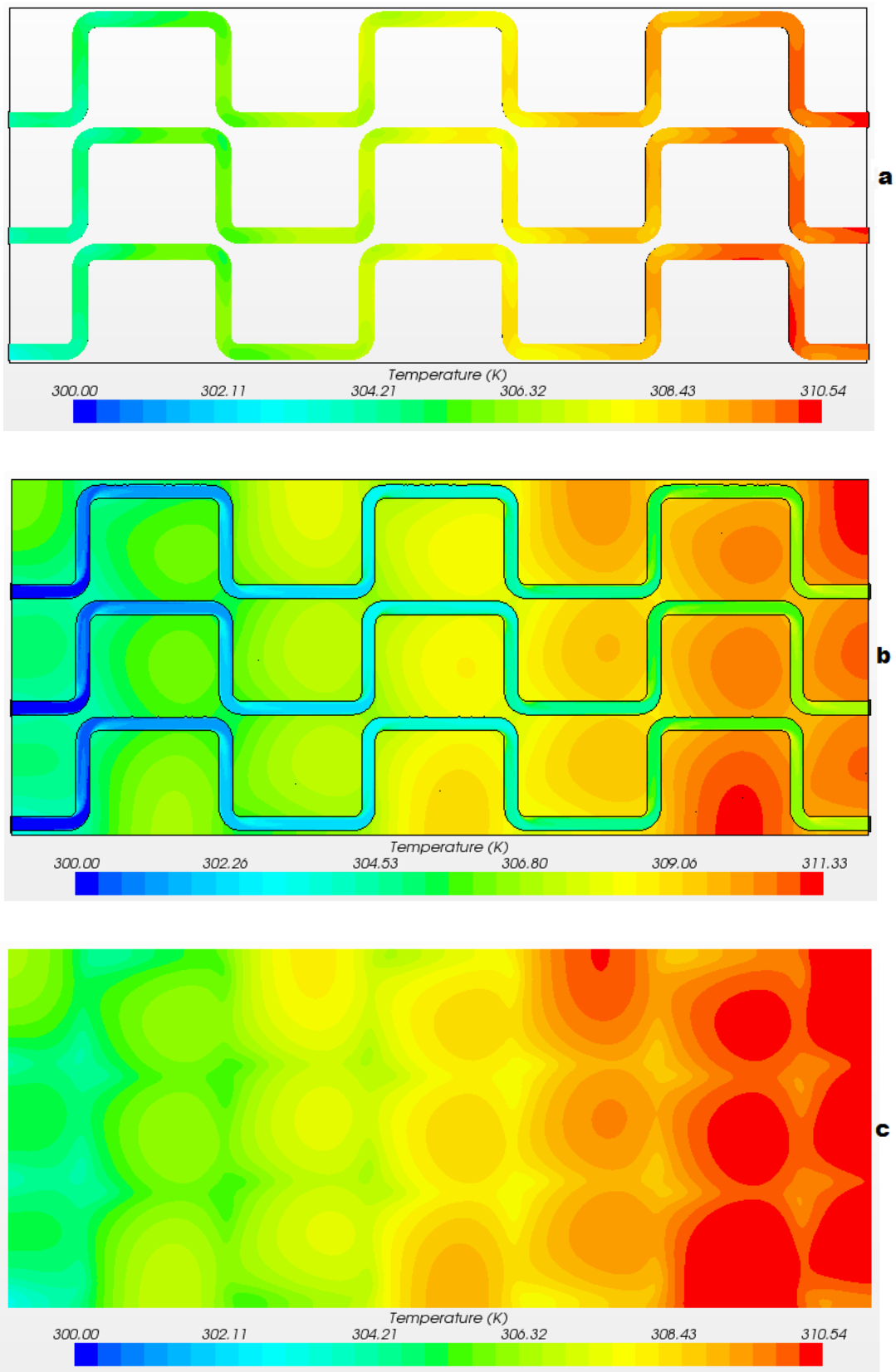

Figure 5-9 - Temperature distributions in the serpentine layout (flow direction from left to right)

Figure 5-9 illustrates the temperature distributions in the serpentine layout with: a) the distributions in the channels, b) the temperature distribution on the plane and c) the temperature distribution on

the surface of the plate. In Figure 5-9 **b** and **c** the heat spots can be seen. It should also be noted that the areas of interest are between the channels and not on the edges of the domain. This is an indication of the areas where material was inefficiently used in terms of heat transfer. Improved stacking abilities resulted in improved area densities which minimized these heat spots to enhance immediate heat transfer.

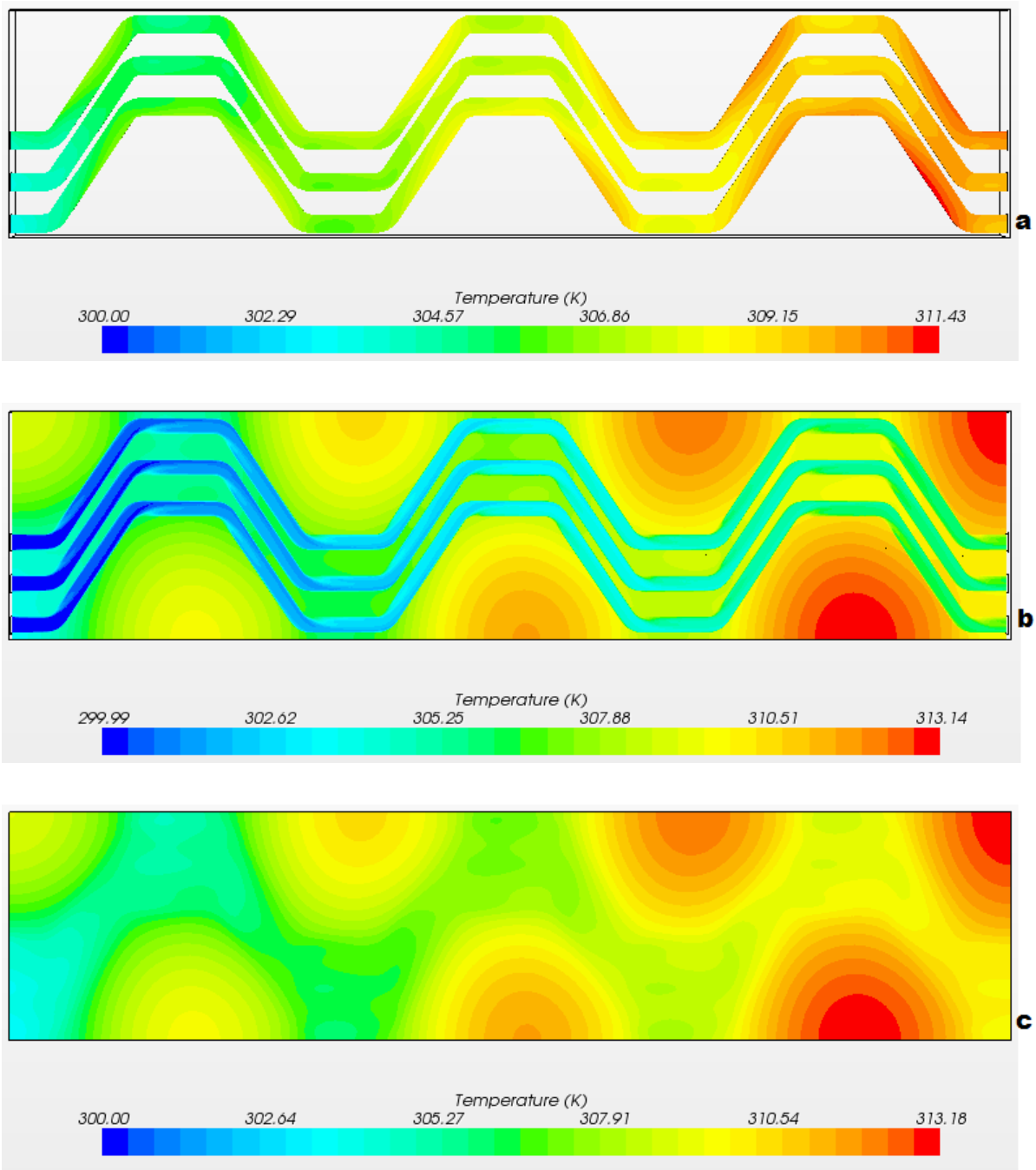

Figure 5-10 - Temperature distribution in the trapezoidal layout (flow direction from left to right)

It can be noted in Figure 5-10 that the heat spots are smaller than those of Figure 5-9. This is due to the better stacking ability of the trapezoidal shape compared with that of the serpentine shape.

The last set of figures represents the temperature distributions within the zigzag layout. This layout yielded the best volume ratio in comparison with serpentine and trapezoidal layouts (the volume ratios of all the layouts will be presented in the next section).

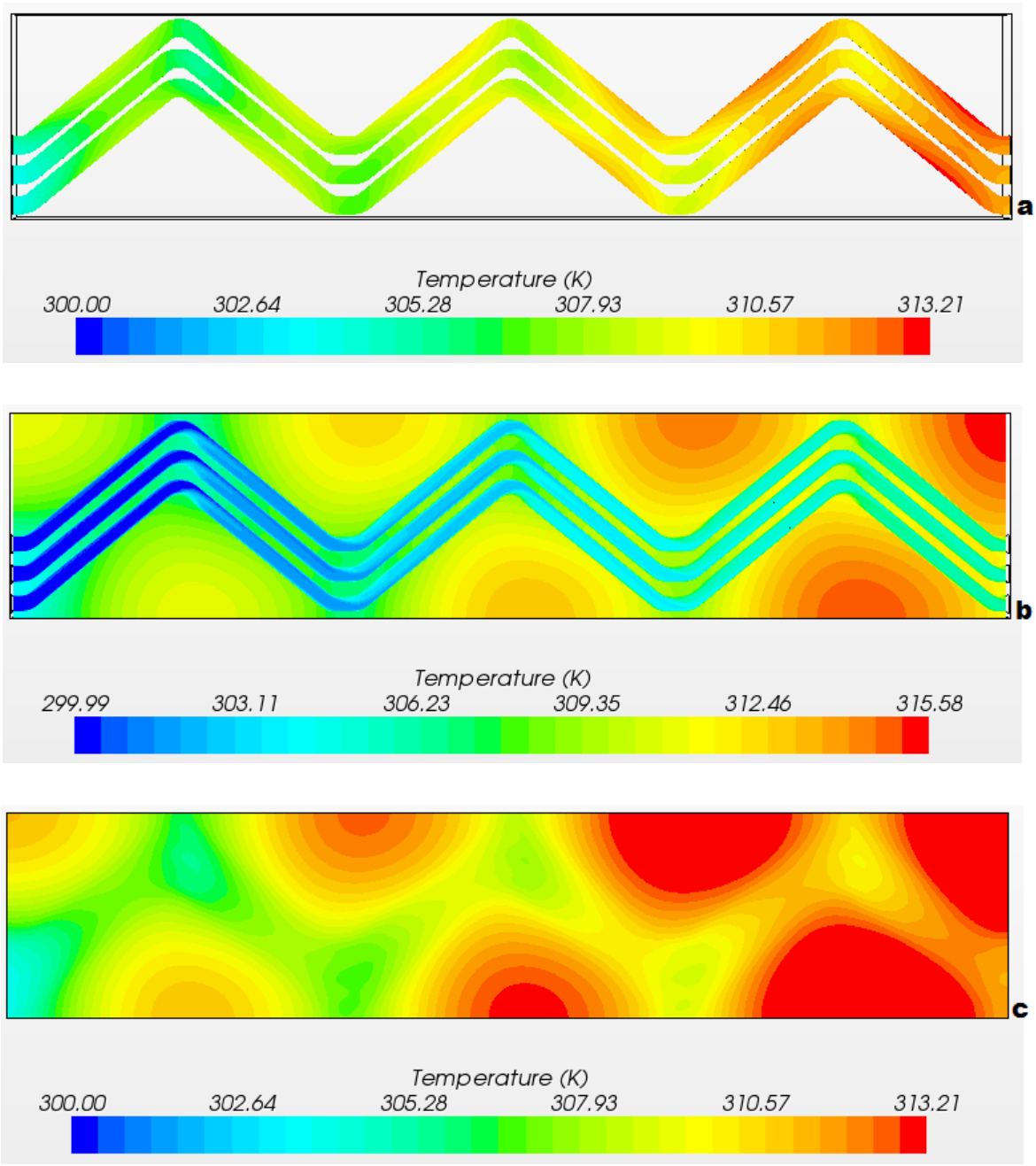

Figure 5-11 - Temperature distribution in the zigzag layout

Figure 5-11 represents the temperature distribution through the zigzag layout. It can be noted than almost no heat spots are present. This is due to the improved stacking ability of the zigzag layout. The next set of figures give the temperature distribution on the plane (as presented Figure 4-4) with regards to the temperature distribution on a line probe located on the plane. This probe line, as stated, was located on the plane in the centre of the second period of the channels. The

temperature difference can be identified as the variance in the temperatures between the solid and the fluid.

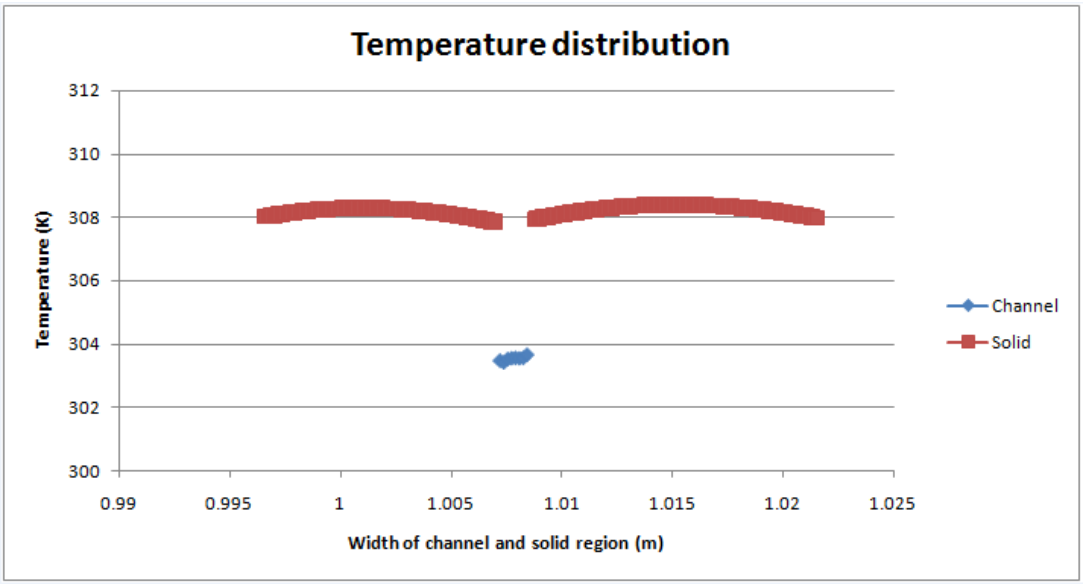

Figure 5-12 - Line probe temperature distribution for serpentine layout

Figure 5-12 shows the temperature distribution within the solid and the fluid for the serpentine layout. The blue diamonds represent the temperature in the fluid while the red squares represent the temperature in the solid. The difference in the temperature should be noted between the internal fluid and the solid. A smaller temperature variation between the solid and the fluid implies that better heat transfer between the regions occurred.

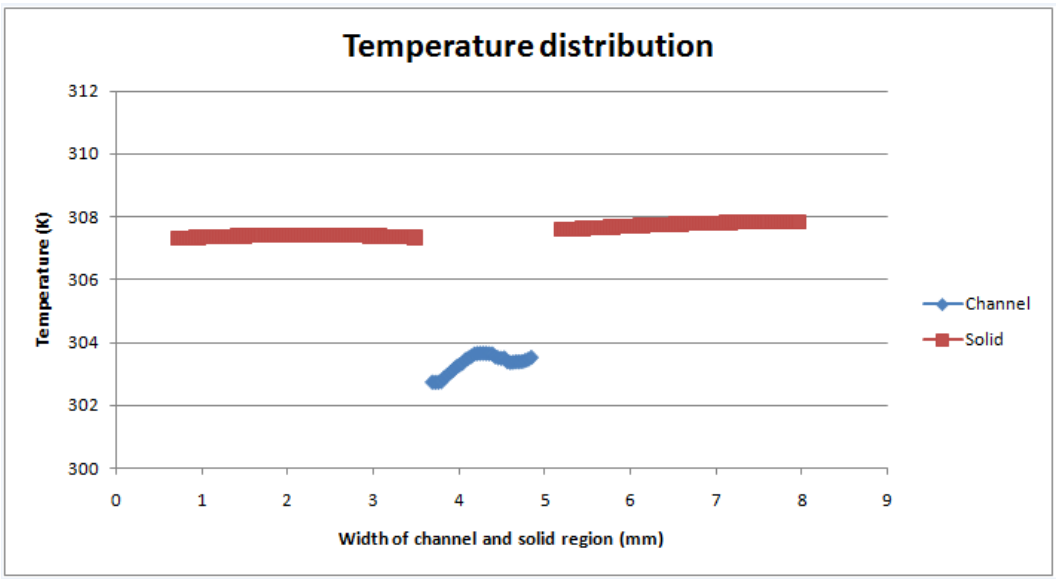

Figure 5-13 - Line probe temperature distribution for trapezoidal layout

Figure 5-13 represents the temperature distribution for the trapezoidal case. The red squares represent the temperature in the solid while the blue diamonds represent the temperature in the fluid. It can already be noted that the average temperatures of the solid in the trapezoidal layout were lower than that of the serpentine layout.

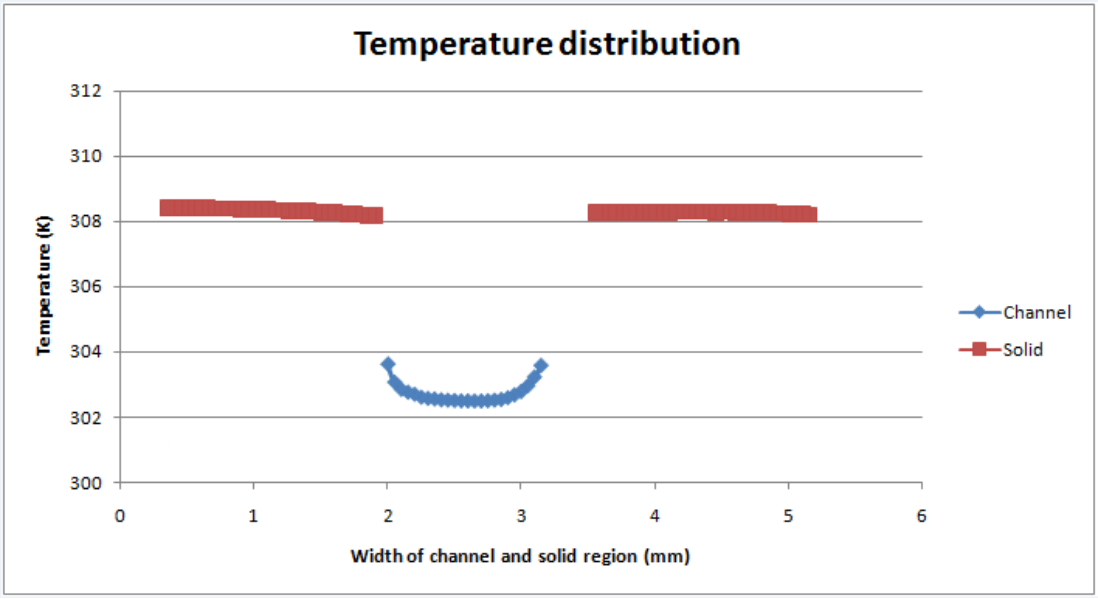

Figure 5-14 - Line probe temperature distribution for zigzag layout

Figure 5-14 gives the temperature distribution for the zigzag shape. The blue diamonds represent the temperature in the fluid region while the red squares represent the temperature in the solid. From the above three figures the differences in the temperatures through the solids and fluid can be seen. Proper conclusions regarding the results for the layouts will follow in the next section.

Details regarding the volume ratios, heat spots and enhancement factors are presented in the next section.

5.2.2. Volume ratios of the configurations

The volume ratios of the layouts were calculated using equation (4.1). The volume ratios for the three test cases are presented in Table 5-5.

Table 5-5 - Comparison of the configurations

	Serpentine	**Trapezoidal**	**Zigzag**
$V_c\ (mm^3)$	90.74	76.54	70.26
$V_s\ (mm^3)$	453.6	181.3	81.86
V_r	0.2001	0.4223	0.8584
Temperature difference (K)	4.65	4.21	5.57
E_f	0.043	0.1003	0.1541

Table 5-5 clearly shows that the zigzag shape has the largest volume ratio of the three cases that were inspected. The volume ratio alone cannot indicate the effectiveness of material usage. This can be noted as the zigzag layout has the best volume ratio but also the largest temperature difference. Table 5-5 also shows the difference between the solid temperatures and the fluid temperatures, presented as the delta spot. The temperature difference is the difference between the average temperature of the solid and the average temperature of the fluid on the line probe. These temperature differences were calculated and presented in Table 5-5 together with the overall enhancement factor.

When comparing these layouts and their results, it can be noted that there are correlations between these findings and that of Figure 2-17: **c**. The heat transfer intensification was determined on geometrical parameters and the heat transfer enhancements of the layouts. The zigzag layout delivered the most promising results and is the case for this study when evaluating against the factors defined in section 4.1.

To therefore make valuable conclusions, the magnitude and the physical size of the heat spots together with the volume ratios should be taken into account. From the three cases the zigzag layout provides the most effective material usage when evaluated according to the enhancement factor.

6 Conclusions and recommendations

6.1. Conclusions

The purpose of the study was to investigate the effect of the surrounding solid material on the heat transfer and temperature distribution inside a CHE using CFD simulations of not only the fluid but the fluid and the solid material.

The software delivered sufficiently accurate results during the validation process where the *T* and *H2* boundary conditions were applied to determine the heat transfer across the solid-fluid-interface.

The effect of the surrounding solid material was defined in terms of the heat spots, the volume ratios, temperature difference and the enhancement factor for the various layouts. The effectivity of test case designs was evaluated according to these parameters. The temperature difference give an indication of the effective material usage in terms of heat transferred and can be useful when transient test cases are simulated including thermal inertia. The conductive heat transfer in the material partly determines these temperature differences.

From the volume ratios it was seen that a higher volume ratio will increase the enhancement factor more significantly. Smaller temperature differences also increases the enhancement factor. Optimizing these two parameters will increase effective material usage in a CHE.

When comparing the effectivity of the material usage with the heat transfer intensification from the literature, it can be noted that there is a close relation between these performance areas. The volume ratio for a zigzag layout is larger than that of the serpentine layout and so is the heat transfer intensification. When comparing the study to the literature (stacking ability based solely on geometries) it can be noted that there is a close relation.

In conclusion the aim of the study was achieved. It is possible to simulate and examine the effect of the surrounding material together with the flow phenomena in the channels, and evaluate different designs according to set parameters. Channel layout configurations can therefore be optimized for effective material usage when evaluating to the factors as set in the study.

6.2. Recommendations

The aim of the study was to investigate the effective material usage using CFD as modelling technique. From the promising results obtained in this study, it is recommended to:

- Expand the configurations: simulate a range of layouts, with the general forms (trapezoidal, serpentine and zigzag) but vary the non-dimensional ratios (A, B, d, L and R_C).

- Simulate for a range of cross-sections (triangular and square). The cross-sections determine heat transfer inside flow channels and would thus have an influence on the temperature distribution in the solid.

- Introduce multiple primary and secondary plates (it should give more realistic results). An assumption was made during this study that a constant heat flux was added to the domain. In real exchangers the flux changes along the axial direction as the temperature difference between primary and secondary sides also change.

- Simulate for a range of Reynolds numbers. Each application has its own set of parameters. To effectively evaluate the performance of a certain application, the parameters must be adjusted accordingly.

- Simulate transient cases and introduce the thermal stress factors. Thermal stresses will also influence and further determine design for effective material usage.

References

CD-ADAPCO. 2011. USER GUIDE - STAR-CCM+ Version 6.02.007.

ERDOğAN, Emin M & IMRAK, Erdem C. 2005. THE EFFECT OF DUCT SHAPE ON THE NUSSELTS NUMBER. *Mathematical and Computational Applications*, 10(1):79-88.

GEYER, Paul E, FLETCHER, David F & HAYNES, Brian S. 2007. Laminar flow and heat transfer in a periodic trapezoidal channel with semi-circular cross-section. *International Journal of Heat and Mass Transfer* , 50(17-18):3471-3480. August.

GUPTA, Raghvendra, GEYER, Paul E, FLETCHER, David F & HAYNES, Brian S. 2008. Thermohydraulic performance of a periodic trapezoidal channel with a traingular cross-section. *International Journal of Heat and Mass Transfer*, 51(11-12):2925-2929. June.

IN HUN, Kim, HEE CHEON, No, JEONG IK, Lee & BYONG GUK, Jeon. 2009. Thermal hydraulic performance analysis of the printed circuit heat exchanger using a helium test facility and CFD simulations. *Nuclear Engineering and Design*:2399-2408.

INCROPERA, Frank P, DEWITT, David P, BERGMAN, Theodore L & LAVINE, Adrienne S. 2006. Fundamentals of Heat and Mass Transfer. Hoboken: John Wiley & Sons.

KAMINSKI, Deborah A & JENSEN, Michael K. 2005. Introduction to Thermal and Fluids Engineering. Hoboken: John Wiley & Sons, Inc.

LAMARSH, John R & BARATTA, Athony J. 2001. Introduction to Nuclear Engineering. New Jersey: Prentice-Hall, Inc.

MLCAK, Justin D, ANAND, N.K & RIGHTLEY, Michael J. 2008. Three-dimensional laminar flow and heat transfer in a parallel array of microchannels etched on a substrate. *International Journal of Heat and Mass Transfer*:5182-5191.

MUNSON, Bruce R & YOUNG, Donald F. 2006. Fundamentals of Fluid Mechanics. Hoboken: John Wiley & Sons.

QU, Weilin, MALA, Gh. Mohiuddin & LI, Dongqing. 2000. Heat transfer for water flow in trapezoidal silicon microchannels. *International Journal of Heat and Mass Transfer*:3925-3936.

ROSAGUTI, Nathan R, FLETCHER, David F & HAYNES, Brian S. 2006. Laminar flow and heat transfer in a periodic serpentine channel with semi-circular cross-section. *International Journal of Heat and Mass Transfer*:2912-2923.

ROSAGUTI, Nathan R, FLETCHER, David F & HAYNES, Brian S. 2007. Low-Reynolds number heat transfer enhancement in sinusoidal channels. *Chemical Engineering Science*, 62(3):694-702. February.

ROUSSEAU, P G & VAN ELDIK, M. 2011. Thermal-Fluid Sytems Modelling I - Lecture Notes. Potchefstroom: North-West University.

SHAH, R.K & LONDON, A.L. 1978. Laminar flow forced convection in ducts. New York: Academic Press.

VENTER, J C. 2010. The optimal hydraulic diameter of semicircular and triangular shaped channels for compact heat exchangers. Potchefstroom: North-West University. 1-41 p.

VERSTEEG, H K & MALALASEKERA, W. 2007. An Introduction to Computational Fluid Dynamics: The Finite Volume Method. Harlow: Pearson Education Limited.